JPET Fast Forward. Published on July 12, 2019 as DOI: 10.1124/jpet.119.258947

Title Page

An inhibitor of fatty acid synthase thioesterase domain with improved cytotoxicity against breast cancer cells and stability in plasma.

Leslie E. Lupien, Evan M. Dunkley, Margaret J. Maloy, Ian B. Lehner, Maxwell G. Foisey, Maddison E. Ouellette, Lionel D. Lewis, Darcy Bates Pooler, William B. Kinlaw, and Paul W. Baures

LEL, WBK: The Geisel School of Medicine at Dartmouth, One Medical Center Drive, Lebanon, NH 03756

LEL: Program in Experimental and Molecular Medicine, Dartmouth College, Dartmouth-Hitchcock Medical Center, One Medical Center Drive, Lebanon, NH 03756

EMD, MJM, IBL, MGF, MEO, PWB: Department of Chemistry, Keene State College, Keene, NH 03435

WBK: Department of Medicine, Division of Endocrinology and Metabolism, Norris Cotton Cancer Center, The Geisel School of Medicine at Dartmouth, Lebanon, NH 03766

LDL, DBP: Section of Clinical Pharmacology & The Clinical Pharmacology Shared Resource, The Geisel School of Medicine at Dartmouth, Lebanon, NH 03766

Running Title Page

a) Improved cytotoxicity and stability of a FASN inhibitor

b) Paul W. Baures

Department of Chemistry

229 Main Street

Keene State College

Keene, NH 03435

Tel: (603)-358-2769

E-mail: pbaures@keene.edu

c) Number of text pages: 65

Number of tables: 1

Number of schemes: 1

Number of figures: 11

Number of references: 92

Number of words in the Abstract: 222

Number of words in the Introduction: 840

Number of words in the Discussion: 1450

d) Abbreviations Employed

BC: breast cancer

CTG: Cell Titer-Glo (viability assay)

FA: fatty acid

FASN: fatty acid synthase

FASNi: FASN inhibitor

FASN-TE: FASN thioesterase domain

LPL: lipoprotein lipase

LPDS: lipoprotein-depleted serum

PI: propidium iodide

e) Recommended Section Assignment

Drug Discovery and Translational Medicine

Abstract

It is well recognized that many cancers are “addicted” to a constant supply of fatty acids (FAs) and exhibit brisk *de novo* FA synthesis. Upregulation of a key lipogenic enzyme, fatty acid synthase (FASN), is a near-universal feature of human cancers and their precursor lesions, and has been associated with chemoresistance, tumor metastasis, and diminished patient survival. FASN inhibition has been shown to be effective in killing cancer cells, but progress in the field has been hindered by off-target effects and poor pharmaceutical properties of candidate compounds. Our initial hit (**1**) was identified from a high-throughput screening effort by the Sanford-Burnham Center for Chemical Genomics using purified FASN thioesterase domain (FASN-TE). Despite being a potent inhibitor of purified FASN-TE, **1** proved highly unstable in mouse plasma and only weakly cytotoxic to breast cancer (BC) cells *in vitro*. An iterative process of synthesis, cytotoxicity testing, and plasma stability assessment was used to identify a new lead (**41**). This lead is more cytotoxic against multiple BC cell lines than (-)-*trans*-C75, the literature standard for inhibiting FASN, is stable in mouse plasma, and shows negligible cytotoxic effects against non-tumorigenic mammary epithelial cells. Compound **41** also has drug-like physical properties based on Lipinski’s Rules and is therefore a valuable new lead for targeting fatty acid synthesis to exploit the requirement of tumor cells for fatty acids.

JPET Fast Forward. Published on July 12, 2019 as DOI: 10.1124/jpet.119.258947

Significance Statement

An iterative process of synthesis and biological testing was used to identify a novel thioesterase domain FASN inhibitor that has drug-like properties, is more cytotoxic to breast cancer cells than the widely used (-)-*trans*-C75, and has negligible effects on the growth and proliferation of non-cancerous mammary epithelial cells. Our studies have confirmed the value of using potent and selective FASN inhibitors in the treatment of BC cells and shown that the availability of exogenous lipoproteins may impact both cancer cell FA metabolism and survival.

JPET Fast Forward. Published on July 12, 2019 as DOI: 10.1124/jpet.119.258947

Introduction

Cancer cells exhibit fundamental metabolic alterations that drive and maintain the malignant phenotype. Since the 1920's it has been known that, in contrast to most normal tissues, cancer cells avidly take up glucose and convert it to lactate through the glycolytic pathway, irrespective of whether oxygen is present (aerobic glycolysis, "Warburg Effect") (Warburg, 1956). Aerobic glycolysis not only provides cancer cells with energy, but also diverts carbon to the synthesis of cellular building blocks, including lipids (Zaidi, 2013). Heightened *de novo* lipid synthesis, mediated through upregulation of the requisite enzymes, including FASN, is considered a near-universal hallmark of most human tumor cells and their precursor lesions (Menendez and Lupu, 2007; Hanahan and Weinberg, 2011; Ward and Thompson, 2012; Benjamin, 2015; Gonzalez-Guerrico, 2016). Increased FASN expression is associated with cancer progression, higher risk of recurrence and metastasis, reduced response to classical chemotherapeutic agents, multi-drug resistance, and diminished patient survival (Rysman, 2010; Liu, 2013; Wu, 2014; Jung, 2015; Heuer, 2017; Menendez and Lupu, 2017).

FASN is a multifunctional, homodimeric enzyme. Each monomer is a large polypeptide comprised of seven catalytic domains working in concert to synthesize the 16-carbon saturated FA palmitate from acetyl-CoA and malonyl-CoA (Buckley, 2017). Palmitate and palmitate-derived lipids have integral roles in cell metabolism, membrane architecture, protein localization, and intracellular signaling (Menendez and Lupu, 2007; Flavin, 2010; Daniels, 2014; Gonzalez-Guerrico, 2016). Studies of the mechanistic role of FASN have revealed that it fuels cancer cell proliferation

and malignant progression by: (1) generating FA precursors required for membrane synthesis and ATP production (Buckley, 2017; Luo, 2017; Jafari, 2019), (2) altering membrane composition and fluidity to confer resistance to endogenous and exogenous insults, including chemotherapy and membrane peroxidative damage (Liu, 2008; Rysman, 2010), (3) modulating the composition of lipid raft membrane microdomains, which house the membrane receptor tyrosine kinases that modulate key cellular processes including signal transduction, intracellular trafficking, cell polarization and migration (Swinnen, 2003; Menendez, 2005), (4) providing palmitate for the covalent post-translational modification (S-acylation, palmitoylation) of tumor-promoting signaling proteins (e.g., Wnt, tubulin, H/N/K-RAS) (Levental, 2010; Anderson and Ragan, 2016; Heuer, 2017), (5) regulating the formation of structures that drive metastasis and invasion (Zaytseva, 2012; Benjamin, 2015; Singh, 2015; Ventura, 2015; Gonzalez-Guerrico, 2016, Wang, 2016; Jafari, 2019), and (6) generating oncogenic signaling lipids, such as diacylglycerol and phosphatidylinositol (Benjamin, 2015; Heuer, 2017; Wagner, 2017). In these various ways, FASN modulates cancer cell proliferation, survival, extracellular matrix organization, migration and invasion, and the expression and activity of signaling networks required for maintaining the malignant phenotype (Menendez and Lupu, 2017).

Participation of FASN in this plethora of cancer-promoting pathways positions the enzyme as an attractive therapeutic target. Pharmacologic or RNAi-mediated inhibition of FASN has been shown to attenuate cancer cell growth, induce apoptosis, and diminish metastatic potential of cancer cells in many

JPET Fast Forward. Published on July 12, 2019 as DOI: 10.1124/jpet.119.258947

different models, while exerting no direct effects on the growth and survival of normal cells (Kuhajda, 1994; Pizer, 1996; De Schrijver, 2003; Kridel, 2004; Menendez and Lupu, 2007; Zaytseva, 2012; Li and Cheng, 2014; Zaytseva, 2014; Ventura, 2015; Rohrig and Schulze, 2016; Buckley, 2017; Menendez and Lupu, 2017). Clinical efficacy of FASN inhibitors (FASNi) alone or in combination therapy has begun to be realized with TVB-2640, a compound developed by 3-V Biosciences (Institute, 2017; Dean, 2016). However, progress in the field continues to be slowed by off-target effects and poor pharmaceutical properties of candidate FASN inhibitors, reviewed in Menendez and Lupu (2007), Flavin, (2010), Liu, (2010), Kinlaw, (2016), Rohrig and Schulze (2016), and Menendez and Lupu (2017). The generation of more potent and selective FASN inhibitors has potential application to a wide range of cancer types and is therefore an important goal.

Imidazole-4,5-dicarboxylic acid is a useful scaffold for drug discovery (Baures, 2009) and has been used to create inhibitors of human immunodeficiency virus protease (Baures, 1999) to target HL-60 promyelocytic leukemia cells (Perchellet, 2005) and in the design of inhibitors of protein-protein interactions (VanCompernolle, 2003). The ability to readily derivatize the scaffold and the conformational behavior resulting from a strong intramolecular hydrogen bond (Baures, 2002; Rush, 2005) were features that enabled the inclusion of these compounds in the Molecular Library Small Molecule Repository (MLSMR) for screening within the NIH Molecular Libraries Initiative (Austin, 2004). A high-throughput bioassay was used to identify inhibitors of the FASN thioesterase domain. This initial screening effort and a series of confirmatory screens identified

JPET Fast Forward. Published on July 12, 2019 as DOI: 10.1124/jpet.119.258947

1 as the most potent inhibitor against this domain from the library of 362,050 compounds. Compound **1** and several closely related derivatives (**Figure 1**) were found to be highly unstable in mouse plasma and demonstrated limited cytotoxicity against BC cells *in vitro.* Multiple rounds of rational modification were used to overcome the stability issues of **1** and generate stable, potent and selective FASNi. The new lead compound reported herein is a structurally unique FASN-TE inhibitor that is more cytotoxic across a panel of BC cell lines than literature standards, such as (-)-C75, and has displayed selectivity for breast cancer cells. These studies have additionally yielded insights into the different pathways that cancer cells use to acquire the FAs that they require.

JPET Fast Forward. Published on July 12, 2019 as DOI: 10.1124/jpet.119.258947

Materials and Methods

General. Reagents were from commercial suppliers and used without additional purification. Solvents were purchased in the highest grade available from Fisher Scientific and passed through a MBRAUN MB-SPS-800 purification system prior to use. Thin layer chromatography (TLC) was performed on 250 μm silica gel plates and compounds were visualized using UV light. Column chromatography was performed on silica gel (Fisher Scientific, Grade 60, 230-400 mesh). Columns were prepared in plastic syringe bodies (130 × 25 mm) filled to 2/3 capacity with silica gel. Fractions containing only the desired product were pooled and concentrated under vacuum. ^{1}H NMR spectra were recorded at 400 MHz in $CDCl_3$ with $CHCl_3$ as the internal reference (δ 7.24) or DMSO-d_6 with DMSO as the internal reference (δ 2.49). The ^{13}C NMR spectrum of **41** was recorded at 100.5 MHz in $CDCl_3$ with $CHCl_3$ as the internal reference (δ 77.00).

Synthesis. Synthesis of **1.4** from **1.1** was performed as shown in **Scheme 1**, as previously described (Solinas, 2008). Briefly, freshly-prepared **1.2** was used in the reaction with lysine derivative **1.3** to give **1.4** as a white or off-white solid following extraction and precipitation. This intermediate can be stored at room temperature indefinitely. Two equivalents of glycine benzyl ester hydrochloride, **1.5**, were added to **1.4** in dichloromethane along with two equivalents of diisopropylethylamine, and the reaction was stirred at room temperature for 16-48 hours. The progress of each reaction was followed with TLC. Purification by column chromatography using a

gradient of hexanes and ethyl acetate afforded **1** as a film with ^{1}H NMR and LC-MS data consistent with that previously reported for this compound (Solinas, 2009). Compounds **11**-**43** were prepared from **1.4** using the same approach and the corresponding amino acid or amine to replace **1.5**. Compounds **15-24** required the synthesis of derivatives of **1.5** that were subsequently used in the reaction. Compounds **11**-**43** were purified by column chromatography using a gradient of hexanes/ethyl acetate or dichloromethane with 3% methanol (v/v). The purity and identity of final products were determined by LC, LC-MS/MS and ^{1}H NMR spectroscopy. Additional details regarding the synthesis and characterization of these derivatives are provided in the Supplemental Data.

LC and LC-MS/MS supporting compound purity and identity. Compounds were analyzed for purity and identity by LC-MS/MS using a Dionex Ultimate 3000 component LC system and Thermo Scientific TSQ Vantage triple quadrupole mass spectrometer (LC-MS/MS) with HESI-II probe operating in positive ion mode. Solutions of the compounds were injected onto a 1.9 μm Hypersil GOLD (50 × 2.1 mm) high-performance liquid chromatography (HPLC) column with a guard column (10 × 2.1 mm) attached at 40°C. Compounds were eluted over 6 min with a gradient of 30-90% CH_3CN and 70-10% H_2O, each containing 0.1% CH_3CO_2H at a 0.75 mL/min flow rate. The column was washed with 90% CH_3CN for 1.5 min at the end of each injection, and then equilibrated with 30% CH_3CN for 1.5 min before each new injection. The mass spectrum was recorded using ESI detection from 50-800 (m/z). In addition, the samples were analyzed for purity on a Polaris 5 μm

JPET Fast Forward. Published on July 12, 2019 as DOI: 10.1124/jpet.119.258947

C18-A (50 × 2.0 mm) HPLC column and eluted with a gradient of CH_3CN/H_2O containing 0.1% CH_3CO_2H at a 0.2 mL/min flow rate. Compounds were detected at 218 nm. The mobile phase gradient was as follows: 0 min., 4:6 CH_3CN/H_2O → 1 min., 4:6 CH_3CN/H_2O → 12 min., 10:0 CH_3CN/H_2O → 13 min., 10:0 CH_3CN/H_2O → 14 min., 4:6 CH_3CN/H_2O → 20 min., 4:6 CH_3CN/H_2O.

Cell lines and tissue culture. MCF-7, MDA-MB-231, BT-474, DU4475, SKBR3 and T47-D breast cancer cells, and HeLa cervical cancer cells were obtained from the American Type Culture Collection (ATCC) and routinely grown in phenol red-containing HyClone RPMI-1640 media with 10% (v/v)-heat-inactivated fetal bovine serum (FBS) (GE Healthcare Life Sciences) and 1% penicillin-streptomycin. Cells were maintained at 37°C in a humidified atmosphere containing 5% CO_2. MCF10A mammary epithelial cells were cultured in DMEM/F12 growth media (Invitrogen) supplemented with 5% horse serum (Invitrogen), 20 ng/mL epidermal growth factor (Peprotech), 0.5 mg/mL hydrocortisone, 100 ng/mL cholera toxin, 10 µg/mL insulin (Sigma) and 1% penicillin-streptomycin. Cell line characteristics are listed in **Table 1**. Lipoprotein-depleted and "matched control" FBS were attained from Kalen Biomedical (Cat. No. 880100; 880170).

Cell viability assays. FASN and lipase inhibitors were purchased from Cayman Chemical (Ann Arbor, Michigan) diluted in DMSO, and stored in the dark at -20°C until use. These included: (-)-*trans*-C75 [tetrahydro-4-methylene-2*S*-octyl-5-oxo-3*R*-furancarboxylic acid] (20 mM stock), cerulenin (20 mM), GSK264220A [N-[2-

methyl-5-(1-piperidinylsulfonyl)-3-furanyl]-N'-phenyl-urea] (50 mM), orlistat (20 mM). Inhibitors were diluted in tissue culture medium immediately before use; control cells were cultured in medium containing the same concentration of DMSO as the highest treatment condition.

Seeding densities for each cell line were determined for each treatment duration to ensure that cells were both capable of logarithmic growth and remained subconfluent at the experimental endpoint. Cells were seeded into 96-well plates, allowed to adhere overnight, treated with freshly-diluted drugs on day 2, and cultured for 72 h prior to assessment. Initial cytotoxicity screens were conducted with MCF-7 BC cells, with cells being treated for 72 h in standard media at concentrations ranging from 5 to 100 μM of inhibitor. Cell viability was assessed using alamarBlue Cell Viability Reagent (Invitrogen), according to manufacturer guidelines. Extended viability screens were carried out using the ATP-based Cell Titer-Glo (CTG) 2.0 Assay (Promega). Luminescence was read using a LMAX II luminometer (Molecular Devices). Background luminescence was calculated from blank/CTG alone wells. Luminescence values (RLU) were normalized to vehicle and compiled as % DMSO control. Half-maximal inhibitory concentration (IC_{50}) determination was performed using a non-linear regression curve-fitting algorithm: log(inhibitor) vs. response-variable slope (four parameter) with Graph Pad Prism 6.0.

Cell death and apoptosis assay. Apoptosis was assessed using a Dead Cell Apoptosis Kit with Annexin V Alexa Fluor 488 and Propidium Iodide (PI)

(ThermoFisher Scientific), according to the manufacturer's instructions. Flow cytometry data was read with the 8-color MACSQuant-10 (Miltenyi Biotec) and analyzed using FlowJo software. Percent apoptosis is shown by the percentage Annexin V+ cells in the population, where total cell death may be calculated as the sum of the Annexin V+/PI+, Annexin V+/PI-, and Annexin V-/PI+ populations.

Statistics. Statistical significance was evaluated using two-tailed unpaired student's t-tests with correction for multiple comparisons (Holm-Sidak method), where applicable, on the means of at least three independent *in vitro* experiments. Values of $p < 0.05$ were deemed significant: $*p < 0.05$, $**p < 0.01$, $***p < 0.001$. Error is presented as mean ± SD.

Plasma stability assay. Each FASN inhibitor (200 nM in a total volume of 50 μL) was tested for stability both in HPLC solvent (70% acetonitrile) and in mouse plasma following a 1 h incubation in several conditions (on ice, 25°C, 37°C). Immediate recovery (no incubation) of compound from plasma at 25°C was also tested. After incubation, 200 μL of acetonitrile containing 80 nM of a stable internal standard (**ILP-III-15**; Supplementary Data Figure S1) was added to each sample. Samples were immediately vortexed and centrifuged at 12,000 rpm for 5 min. Supernatants were dried under nitrogen at 45°C, resuspended in 50 μL 70% acetonitrile and transferred to the autosampler where 5 μL were injected for LC-MS/MS analysis.

JPET Fast Forward. Published on July 12, 2019 as DOI: 10.1124/jpet.119.258947

Stability analysis by LC-MS/MS. Samples were injected onto a 50 x 2.1 mm, 1.9 micron Hypersil GOLD column fitted with a 10 × 2.1 mm C18 guard at 40°C. Isocratic elutions were achieved with 60% acetonitrile, 40% water and 0.1% acetic acid at a rate of 0.75 mL/min on the Dionex/Thermo LC-MS/MS system. Mass spectrometry parameters were: spray voltage 3750 V, vaporizer temperature 474°C, capillary temperature 202°C, sheath gas pressure 30 and auxiliary gas pressure 25. Selected reaction monitoring, collision energy, and SLens parameters were tuned selectively for each compound.

Analysis of compound stability. We defined stability as recovery of $\geq$ 70% of compound from mouse plasma after a 1 h incubation at 37°C. Recovery was considered with respect to drug in solvent or plasma on ice (presumed to be most stable conditions) vs. plasma at 37°C. Some compounds may have been subject to enzymatic degradation in the plasma, while others may have bound covalently to plasma proteins.

Malonyl-CoA LC-MS/MS assay. BT-474 BC cells were treated with FASNi (50 μM) for 4 h in standard RPMI-1640 media, washed with PBS, harvested with trypsin, and frozen as cell pellets at -20°C. Cell pellets were resuspended at 10,000 cells/μL in cold 40:40:20 acetonitrile:methanol:water containing 1 μg/mL ^{13}C-malonyl-CoA internal standard. Calibrator and quality control samples were made in 40:40:20 acetonitrile:methanol:water containing internal standard. All samples were vortexed and centrifuged 4,300 x g for 20 min at 4°C. Supernatants were

collected and 25 µL injected onto a Dionex Ultimate 3000 HPLC system in tandem with a TSQ Vantage mass spectrometer. HPLC separation was achieved with a gradient of 5→95% methanol, 95→5% 5 mM ammonium acetate over 3 min with a flow rate of 0.3 mL/min on a 40°C Phenomenex Luna C18 2.1 x 50 mm, 1.6 micron column with 2.1 x 10 mm C18 guard cartridge. The mass spectrometer was operated in positive ion mode using a HESI-II probe, with spray voltage 3750 V, vaporizer and capillary temperatures at 380°C and 241°C, respectively, and sheath and auxiliary gases at 20 and 5, respectively. Single reaction monitoring mode was used for the following ion transitions: malonyl-CoA 854.055→303.040 m/z with S-Lens 191 and collision energy 35, 13-C-malonyl-CoA 857.061→350.090 m/z with S-Lens 187 and collision energy 29. The calibration curve was linear over the concentration range 0.01-5 µg/mL, with all quality controls having a CV < 15%.

His_6-FASN-TE protein expression and purification. A pET15b plasmid coding a *N*-terminal His_6-tagged thioesterase domain of FASN (His_6-FASN-TE), with a thrombin recognition sequence separating the His_6 tag from the FASN-TE, was generously provided by W. Todd Lowther (Wake Forest University). This was used for the protein expression and purification of FASN-TE with slight modification from a previously described procedure (Pemble IV, 2007). We used a solution of Bacterial Protein Extraction Reagent (B-PER, Thermo Scientific) with lysozyme and DNase I at a ratio of 5 mL/g of cells to lyse cells. Following the addition of streptavidin-agarose (Thermo Scientific) to remove the biotinylated-thrombin, the

JPET Fast Forward. Published on July 12, 2019 as DOI: 10.1124/jpet.119.258947

protein solution was passed through Ni^{2+}-sepharose and the cleaved protein was collected in the flow-through. This step on Ni^{2+}-sepharose ensured that no residual His_6-FASN-TE remained in the protein solution. The FASN-TE was dialyzed into 20 mM HEPES, pH 7.5, 100 mM NaCl, and 1 mM DTT. For the enzyme assays, the protein was diluted H_2O and dialyzed against 25 mM HEPES, pH 7.5, 12.5 mM NaCl, 0.001% Brij35, and 125 mM sarcosine, resulting in a stock protein concentration of 2.6 mg/mL (75 μM). A 0.71 M TCEP [tris-(2-carboxyethyl)phosphine] stock solution was used to yield a 1 mM TCEP concentration to protect cysteines from oxidation.

FASN-TE Inhibition Experiments. Prior to each experiment, stock protein was diluted to 7.5 μM with 200 mM Tris, pH 7.5, 100 mM NaCl, 0.01% Brij35, and 1.0 M sarcosine. The FASN-TE was used to conduct IC_{50} determinations using 4-methylumbelliferyl heptanoate (Sigma Aldrich) as the substrate with enzyme alone versus solutions of varying concentrations of **1** and **41**. A stock solution of **41** was prepared in 25 mM in DMSO, while a stock solution of **1** was prepared at 6.25 mM in DMSO. Serial dilutions of the stocks were prepared, and 1.0 μL of each was added to 155 μL of the pooled enzyme solution. A DMSO control was prepared analogously. These solutions were incubated for 30 minutes at room temperature before adding 50 μL from each into 3 wells of a 96-well plate (Costar black polystyrene, round bottom). A substrate stock concentration was prepared at 100 mM in DMSO and diluted to 60 μM in water containing 10% DMSO prior to the assay. To each well containing enzyme with or without an inhibitor was then added

JPET Fast Forward. Published on July 12, 2019 as DOI: 10.1124/jpet.119.258947

50 μL of the substrate solution, giving a final substrate concentration of 30 μM. The final enzyme concentration in the assay was 3.75 μM. The final concentrations of **1** in the enzyme assay were 20, 10 , 5, 2.5, 1.25, 0.625, 0.313, 0.156, 0.078, and 0.039 μM, respectively. The final concentrations of **41** in the enzyme assay were 80, 40, 20, 10, 5, 2.5, 1.25, 0.625, 0.313, and 0.156 μM. The plate was shaken for 10 seconds and fluorescence was recorded (360/40 ex, 460/40 em), repeating the shaking and reading every minute for 4 hours. In the absence of inhibitors, the fluorescence reached a maximum in approximately 60 minutes. The background signal resulting from the non-enzymatic hydrolysis of the substrate was subtracted from enzyme plus substrate alone control solution and all of the wells that contained **1** or **41**. Initial velocities were determined at or prior to the point that 10% substrate hydrolysis was evident as determined by the percentage of the maximum fluorescence intensity. Data for each concentration were collected in triplicate, and three experiments were used to determine an average IC_{50} curve for **1** and **41**. Half-maximal inhibitory concentration (IC_{50}) determination was performed using a non-linear regression curve-fitting algorithm: log(inhibitor) vs. response-variable slope (four parameter) with Graph Pad Prism 6.0.

JPET Fast Forward. Published on July 12, 2019 as DOI: 10.1124/jpet.119.258947

Results

Synthesis. The methodology for synthesizing compounds **1**-**10** has been previously reported (Perchellet, 2005; Solinas, 2008; Solinas, 2009); these methods were also used in the synthesis of **11**-**43** (**Scheme 1**). The millimolar scale for the synthesis of **11**-**43**, the TLC eluant and R_f value, as well as the yield of purified compounds are shown in Supplemental Data Table S1. The synthetic procedures and details for reaction intermediates, the reaction scheme, structures, ^{1}H NMR spectra, and LC-MS analysis are also provided (Supplemental Scheme S1, Figures S2-S18, Table S2). Compounds **11**-**43** were characterized by ^{1}H NMR spectroscopy, ^{13}C NMR spectroscopy (**41** only) and LC-MS using total ion count (Supplemental Figures S19-S85). Additional HPLC traces with UV detection at 218 nm to assess for purity are shown (Supplemental Figures S86-S118).

Rational design of structurally-related compounds to improve the stability and *in vitro* cytotoxicity of 1.

Modifications of the benzyl ester moiety. Compound **1** was weakly cytotoxic to MCF-7 BC cells (IC_{50} = 117 μM, Supplementary Figure S120) and was unstable in mouse plasma (0% recovery, < 5 minutes). Heat inactivation of mouse plasma abrogated the instability of **1**, suggesting the presence of esterase or protease activity. We hypothesized that the lability in mouse plasma was due to the benzyl ester bond based on this evidence and the fact that amino acid derivatives like **2**, containing *tert*-butyl esters, were recovered at higher percentages (30-59%) from mouse plasma after 1 h at 37°C (data not shown). Replacing the glycine benzyl

JPET Fast Forward. Published on July 12, 2019 as DOI: 10.1124/jpet.119.258947

ester moiety in **1** for a leucine *tert*-butyl ester resulted in complete recovery of the compound (**ILP-III-15**) from mouse plasma. This leucine derivative was thus used as the internal standard for our compound stability assay (Supplemental Figure S1).

Our design, synthesis, and testing efforts started with the most active hit, **1**, and focused on improving the stability of the benzyl ester bond. This led to derivatives **11**-**14** that replaced part or all of the benzyl ester (**Figure 2A**). Each of these derivatives was substantially more cytotoxic against MCF-7 BC cells *in vitro* than **1** (IC_{50} values ranging from 8-25 μM), but only **13** showed marked improvement in plasma stability (40% recovery after 1 h at 37°C) (**Figure 2B**, **C**). The less than complete recovery of **13** suggested that another activity such as hydrolysis of the glycine amide bond in **1** was possible. A second approach to blocking the action of the protease/esterase activity against these compounds was thus employed. The benzyl ester was modified with an amide bond (**15**) and coupled to steric bulk at the amide nitrogen (**16**), the benzyl carbon (**17**, **18**), or the α-carbon of the amino acid (**19**, **20**) (**Figure 3**). Compound **16** was recovered at only 29% from 37°C plasma after 1 h, and the addition of steric bulk did not improve the cytotoxicity of the compounds (data not shown). Combining a methyl group at the amide nitrogen with one at the α-carbon of the amino acid (**21**, **22**) or the benzyl carbon (**23**, **24**) likewise showed no improvement in the cytotoxicity (data not shown), leading us to abandon this series.

JPET Fast Forward. Published on July 12, 2019 as DOI: 10.1124/jpet.119.258947

The benzylamine series. Benzylamine derivative **25** was flagged as active in the initial high-throughput screen with purified FASN-TE,[2] and also formed the base structure of **13**, which demonstrated improved cytotoxicity in our assays. Compounds based on a substituted benzylamine (**26**-**37**) were thus prepared and tested. Substituents on the aromatic ring impacted both the cytotoxicity and the plasma stability, however, even the more potent of these compounds was not sufficiently stable to justify further investigation (**Figure 4**).

Cyclohexylamine derivatives. Compound **9** demonstrated activity against purified FASN-TE in initial confirmatory assays[3] (FASN-TE IC_{50} = 1.56 μM). While the potency of **9** was approximately 10-fold less than **1** (FASN-TE IC_{50} < 0.16 μM), this compound demonstrated greater plasma stability than other initial hits and was therefore used as inspiration for a series of cyclohexylamine derivatives (**Figure 5**). A boost in the cytotoxicity (IC_{50} ~ 16-24 μM) and plasma stability (90% recovery after 1 h at 37°C) was observed for **38** when the substituent was just a cyclohexylamine. The improvement in cytotoxicity observed for the benzylamine series when an alkyl group was added at the 4-position (**34**-**36**) led us to synthesize the racemic *cis*- and *trans*-4-*tert*-butylcyclohexylamine derivative, **39**. This modification further improved cytotoxicity (IC_{50} ~ 7-16 μM), with plasma stability of 80%. The diastereomeric *cis* and *trans* isomers, **40** and **41**, were prepared for comparison. Both diastereomers were equally cytotoxic to BC cells (~14-18 μM), however, the *cis* isomer (**40**) was recovered at 62%, while the *trans* isomer (**41**) was 98% recovered from mouse plasma. Diastereomers **42** and **43** were

JPET Fast Forward. Published on July 12, 2019 as DOI: 10.1124/jpet.119.258947

comparable in cytotoxicity to **41** but demonstrated far less stability in mouse plasma (**Figure 5**).

The four most promising compounds from this series (**38**, **39**, **41**, **42**) were directly compared in terms of cytotoxicity and plasma stability (**Figure 6**). It was on the bases of these cytotoxicity and stability results, and structural considerations, that compound **41** was chosen as the new lead compound for extended studies.

Extended characterization of a new lead, 41. The ability of **41** to directly bind and inhibit FASN was assessed using a malonyl-CoA LC-MS/MS assay. Treatment of BT-474 BC cells with **41** (4 h, 50 μM) resulted in a significant accumulation of the committed substrate of *de novo* lipogenesis, malonyl-CoA (**Figure 7A**). The identity of **41** as a FASNi targeting the TE domain was next confirmed using a FASN-TE enzyme activity assay. Here, both **1** and **41** displayed concentration-dependent FASN-TE enzyme inhibition compared to hydrolysis observed with substrate alone (with data corrected for non-enzymatic hydrolysis of the substrate) (**Figure 7B**). Together, these data show that **41** binds and inhibits FASN-TE, resulting both in reduced thioesterase enzyme activity and accumulation of the cytotoxic substrate, malonyl-CoA.

Cytotoxicity of **41** was compared to the FASNi (-)-C75 following 72 h continuous treatment in standard media (**Figure 8**). The cytotoxic effects of **41** exceed those observed with treatment of (-)-C75 across BC cell lines (**Figure 8A**, **B**). The FASNi-mediated changes in cell viability could be attributable to a mix of growth inhibition or cytostasis and cell death. Cells were thus stained with Annexin

JPET Fast Forward. Published on July 12, 2019 as DOI: 10.1124/jpet.119.258947

V Alexa Fluor 488 and PI and assessed by flow cytometry following 72 h continuous treatment to quantify FASNi induced apoptosis, more specifically. FASN inhibition resulted in significant concentration-dependent apoptosis in BC cells, with the impact of **41** exceeding that of (-)-C75 at equimolar concentration (**Figure 8C, D**).

Compound **41** exhibited minimal cytotoxic effects against non-tumorigenic MCF10A mammary epithelial cells, creating the potential for a large therapeutic window (**Figure 8E, F**). This is in contrast to other FASNi, including (-)-C75 and cerulenin, where substantial cytotoxicity was observed against MCF10A cells at high concentrations. Effects of **41** and other FASNi were validated using several different measures of cell viability including the Cell Titer-Glo ATP-based assessment (reported here), the DNA-based Hoechst Assay, the protein-based sulforhodamine B (SRB) assay, and the alamarBlue redox indicator (used for initial profiling studies, **Figures 2**-**5**) (data not shown).

The cytotoxic effects of FASNi treatment are concentration-dependent, time-dependent (Supplemental Figure S121), and are impacted by the availability of exogenous lipoproteins in the media (**Figure 9**). This latter observation conforms with previous publications (Kuemmerle, 2011; Zaidi, 2012; Zaidi, Lupien, 2013; Daniels, 2014; Schug, 2015; Svensson, 2016; Cao, 2017) and underscores the importance of *both* endogenous and exogenous FA sources for cancer cell survival and proliferation.

With this in mind, we next investigated the potential of targeting FA synthesis and exogenous FA uptake simultaneously using our FASNi **41** and

JPET Fast Forward. Published on July 12, 2019 as DOI: 10.1124/jpet.119.258947

GSK264220A (GSK), a urea-based inhibitor of lipoprotein lipase (LPL) and endothelial lipase (LIPG) (Keller, 2008; Nomura, 2016). LPL is the major enzyme for extracellular hydrolysis of triglyceride transported in lipoprotein particles, and thus renders this source of fatty acids accessible to cells (Kuemmerle, 2011; Kinlaw, 2016). Concentration-dependent cytotoxicity was observed when BC cells were treated with GSK continuously for 72 h, with most effects on viability observed at concentrations greater than 25 μM (**Figure 10A**). Combined treatment with GSK and **41** caused increased cytotoxicity over either drug alone (**Figure 10B**). We hypothesized that the cytotoxic effects of lipogenesis and lipolysis inhibition might additionally be augmented by removing lipoprotein substrates from the media, and found that this was, in fact, the case. MDA-MB-231 cells cultured in 10% lipoprotein-depleted FBS media and treated with a combination of **41** and GSK264220A (100 μM) showed increased cytotoxicity over **41** alone, or the combination in media containing lipoproteins (**Figure 10C**).

JPET Fast Forward. Published on July 12, 2019 as DOI: 10.1124/jpet.119.258947

Discussion

Here we have summarized the stepwise process through which **41** was rationally designed, established its efficacy against cancer cell lines *in vitro*, and highlighted the therapeutic potential of targeting fatty acid synthesis in breast cancer cells through FASN-TE. Initial screening data that yielded hits **1**-**10** was useful, both in providing basic structure-activity relationship data for inhibition of purified FASN-TE and in offering clues for how to modify **1** to improve cytotoxicity and plasma stability. The fact that heat-denatured plasma led to improved stability of **1** pointed to the action of an esterase or protease. We hypothesized that the lability in mouse plasma was predominantly due to the benzyl ester bond and showed that replacing the glycine benzyl ester moiety in **1** for a leucine *tert*-butyl ester (**ILP-III-15**) resulted in complete recovery of the compound from mouse plasma.

An important goal at the start of this project was to obtain a compound in this structural class worthy of investigating in a mouse model of BC and thereby gauge the suitability of FASN-TE inhibitors for further development. The plasma stability of **1** was therefore an important issue to solve and led us to prepare derivatives **11**-**14** that replaced all or part of the benzyl ester. Each of these derivatives was substantially more cytotoxic against MCF-7 BC cells than **1** (IC_{50} = 117 μM, Supporting Figure S120), however, only **13** showed an improvement in plasma stability. The stability of **13** was similar to that of **2**, further supporting the hypothesis that lack of metabolic stability results in part from hydrolysis of the glycine amide bond of **1**. The biphenyl substructure in **13** and **14** is a privileged

JPET Fast Forward. Published on July 12, 2019 as DOI: 10.1124/jpet.119.258947

scaffold found both in compounds that bind multiple proteins (Hajduk, 2000) and in compounds known to be FA mimetics (Proschak, 2017). Thus, while **13** was a valuable intermediary in testing the significance of the benzyl ester bond to plasma stability, we did not think it represented an optimal structure to move forward.

We simultaneously prepared derivatives **15**-**24** with the dual goal of blocking the action of the protease/esterase activity by adding methyl groups as steric bulk and potentially improving the stability and drug-like properties of the compounds – effects that have been tied to the *N*-methylation of peptides (Biron, 2008). No improvements in cytotoxicity were observed with **15**-**24**, leading us to discontinue this series.

Benzylamine derivative **25** was flagged as active in the initial high-throughput screen with the purified thioesterase domain,[2] and since it also formed the base structure of **13**, a series of benzylamine derivatives (**25**-**37**) were prepared. The plasma stability of **25** was comparable to **13** at room temperature or on ice, but lower at 37°C (Supplemental Data Table S2). Addition of a methyl group at the amide nitrogen (**26**) improved recovery from plasma to 65% at 37°C, but **26** was still not as cytotoxic as **13**. Either the cytotoxicity, the plasma stability, or both were reasons enough for **27**-**37** to be uninteresting, and this series was subsequently abandoned.

Compound **9** was active in the confirmatory assays,[3] albeit approximately 10 times less potent (IC_{50} = 1.56 μM) at the purified TE domain as compared to **1** (IC_{50} < 0.16 μM). Yet, **9** showed improved plasma stability compared with other initial hits and therefore used as inspiration for a series of cyclohexylamine

JPET Fast Forward. Published on July 12, 2019 as DOI: 10.1124/jpet.119.258947

derivatives (**Figure 5**). A boost in the cytotoxicity (IC_{50} ~ 16-24 μM) and plasma stability (90% recovery after 1 h at 37°C) was observed for **38**, when the substituent was a cyclohexylamine alone. The racemic *cis*- and *trans*-4-*tert*-butylcyclohexylamine was both commercially available and relatively inexpensive, and was therefore used to synthesize **39** in order to assess whether cytotoxicity gains could be made, as observed in the benzylamine series between **25** and **35**. This was indeed the case, and the mixture of diastereomers only demonstrated a small decrease in plasma stability compared to **39**. We reasoned the cytotoxicity and plasma stability should be different for the two diastereomers in **39**, so we next synthesized the individual diastereomers **40** and **41** in order to make the comparison. The *trans* stereoisomer, **41**, had superior plasma stability and cytotoxicity against BC cells than that of the *cis* stereoisomer, **40**. A second pair of diastereomeric cyclohexylamine derivatives, **42** and **43**, were prepared to further probe for any increase in cytotoxicity. However, both diastereomers **42** and **43** were comparable in cytotoxicity to **41** and were far less stable in mouse plasma.

Compound **41** was selected for further investigation on the basis of its promising stability and cytotoxicity parameters (**Figures 6, 8**), the fact that substituted cyclohexylamines are not readily available or prepared, and that there was no obvious structure-activity information from another series to suggest what modifications could be made to pursue additional gains in cytotoxicity. Compound **41** was verified as having on-target inhibitory effects against FASN-TE using a malonyl-CoA accumulation assay and a FASN-TE enzyme activity assay (**Figure 7**). To further evaluate **41**, we used a range of breast cancer cell lines that varied

JPET Fast Forward. Published on July 12, 2019 as DOI: 10.1124/jpet.119.258947

by tumor type and biomarker status (ER, PR, HER2) (**Table 1**). Importantly, **41** demonstrated concentration-dependent cytotoxicity across this panel of BC cell lines, was more potent than (-)-C75, and also more selective than classical FASNi, as evidenced by negligible cytotoxicity against the non-tumorigenic mammary epithelial MCF10A cell line.

This new lead compound represents an improved FASNi to investigate the importance of this target in BC. We have shown that **41** is stable in mouse plasma and more cytotoxic across a wide array of BC cell lines than other widely used FASNi. Compound **41** has drug-like properties and structure, making it a promising lead for continued development towards a clinical therapeutic. Valuable guidelines for drug discovery include the rule-of-5 set of properties (Lipinski, 1997; Lipinski, 2000; Lipinski, 2004), the number of rotatable bonds (Veber, 2002), and cell permeability (Egan, 2000). Villoutreix and coworkers used these rules and others to create an online screening tool for filtering lead compounds against the adsorption, distribution, metabolism, excretion, and toxicity (ADME-Tox) properties, thereby facilitating decision making at early stages of drug discovery (Lagorce, 2008; Lagorce, 2018). Importantly, **41** has no major issues related to these filters (**Figure 11**). Only the rotatable bonds are outside of the parameters favored for small-molecule drug discovery, while the intramolecular hydrogen bond formed in this scaffold is recognized as a beneficial feature in the design of orally available drugs (Doak, 2014).

In addition to the insights into the inhibition of the FASN-TE domain provided by this work, important pathophysiological information regarding the role

of lipogenesis in breast cancer biology has also emerged. The “addiction” of several types of cancer cells to fatty acid synthesis is well-recognized (Menendez and Lupu, 2007; Baenke, 2013; Rohrig and Schulze, 2016). We and others have previously reported that, in addition to *de novo* FA synthesis, the uptake of exogenous lipids may provide an alternative source of FA to cancer cells (Ruby, 2010; Kuemmerle, 2011, Zaidi, 2013; Rozovski, 2015; Rozovski, 2016; Cao, 2017; Rozovski, 2018), and that this process is facilitated by the expression of LPL and the cell surface FA uptake channel, CD36. This prompts the hypothesis that cancer cells may occupy various positions along a spectrum of dependence upon FASN-mediated lipogenesis and LPL-driven lipolysis to satisfy their requirement for FA. In the case of prostate cancer cells, recent findings of Swinnen and coworkers further demonstrate that the balance between the two modes of lipid acquisition may be fluid, with the removal of exogenous lipoproteins eliciting increased expression of genes involved in FA synthesis, including FASN (Daniels, 2014). Our current finding that sensitivity to FASN-TE inhibition is enhanced by either inhibition of lipase activity and/or by removal of lipoproteins from tissue culture media strongly supports the concept that FA synthesis and uptake both support BC cell survival. This notion has begun to be realized across a variety of different cancer types, including not only BC (Kuemmerle, 2011; Song, 2012; Slebe, 2016), but also colorectal cancer (Notarnicola, 2012; Tang, 2012), prostate cancer (Wang, 1995; Cerhan, 1997; Connolly, 1997; Fair, 1997; Tokuda, 2003; Brown, 2006; Gazi, 2007; Narita, 2008), hepatocellular carcinoma (Li, 2016; Cao, 2017), lung

JPET Fast Forward. Published on July 12, 2019 as DOI: 10.1124/jpet.119.258947

cancer (Sundaram, 2018), and pancreatic cancer (Vasseur and Guillaumond, 2016).

Several groups have linked obesity or high-fat diets to cancer prognosis, as well as implicated tumor-adjacent adipocytes in altering the metabolism, growth and progression of solid tumors (Tokuda, 2003; Gazi, 2007; Notarnicola, 2012; Nieman, 2013; Abel, 2014; Massa, 2016; Cozzo, 2017; Gonzalez-Reyes, 2018; Luo, 2018). It thus appears that, at least for some tumors, simultaneous targeting of both lipogenesis and uptake/lipolysis will provide the largest anticancer effect. The importance of interactions between these complementary pathways will come into sharper focus as increasingly potent and specific FASN inhibitors, such as compound **41** and its derivatives, become available.

JPET Fast Forward. Published on July 12, 2019 as DOI: 10.1124/jpet.119.258947

Acknowledgements

The authors thank W. Todd Lowther (Wake Forest University) for the plasmid coding the *N*-terminal His_6-tagged thioesterase domain of FASN.

Authorship Contributions

Participated in research design: Lupien, Lewis, Bates Pooler, Kinlaw, Baures

Conducted experiments: Lupien, Dunkley, Maloy, Lehner, Foisey, Ouellette, Bates Pooler, Baures,

Contributed new reagents or analytic tools: Lewis

Performed data analysis: Lupien, Lewis, Bates Pooler, Baures

Wrote or contributed to the writing of the manuscript: Lupien, Lewis, Bates Pooler, Kinlaw, Baures

References

Abel S, Riedel S, and Gelderblom WCA (2014) Dietary PUFA and cancer. *Proc Nutr Soc* **73**: 361-367.

Anderson AM and Ragan MA (2016) Palmitoylation: a protein S-acylation with implications for breast cancer. *NPJ Breast Cancer* **2**: 16028.

Austin CP, Brady LS, Insel TR, and Collins FS (2004) NIH molecular libraries initiative. *Science* **306**: 1138-1139.

Baenke F, Peck B, Miess H, and Schulze A. (2013) Hooked on fat: the role of lipid synthesis in cancer metabolism and tumour development. *Dis Model Mech* **6**: 1353-1363.

Baures PW (1999) Heterocyclic HIV-1 protease inhibitors. *Org Lett* **1**: 249-252.

Baures PW, Rush JR, Wiznycia AV, Desper J, Helfrich BA, and Beatty AM (2002) Intramolecular hydrogen bonding and intermolecular dimerization in the crystal structures of imidazole-4, 5-dicarboxylic acid derivatives. *Crys Growth & Des* **2**: 653-664.

Baures PW (2009) Imidazole-4,5-dicarboxylic acid: A versatile scaffold for drug discovery and materials research. *Trends Heterocyclic Chem* **11**: 1-22.

Benjamin DI, Li DS, Lowe W, Heuer T, Kemble G, and Nomura DK (2015) Diacylglycerol metabolism and signaling is a driving force underlying FASN inhibitor sensitivity in cancer cells. *ACS Chem Biol* **10**: 1616-1623.

Biron E, Chatterjee J, Ovadia O, Langenegger D, Brueggen J, Hoyer D, Schmid HA, Jelinek R, Gilon C, and Hoffman A (2008) Improving oral bioavailability

of peptides by multiple *N*-methylation: somatostatin analogues. *Angew Chem Int Ed* **47**: 2595-2599.

Brown MD, Hart CA, Gazi E, Bagley S, and Clarke NW (2006) Promotion of prostatic metastatic migration towards human bone marrow stoma by Omega 6 and its inhibition by Omega 3 PUFAs. *Br J Cancer* **94**: 842-853.

Buckley D, Duke G, Heuer TS, O'Farrell M, Wagman AS, McCulloch W, and Kemble G (2017) Fatty acid synthase - Modern tumor cell biology insights into a classical oncology target. *Pharmacol Ther* **177**: 23-31.

Cao D, Song X, Che L, Li X, Pilo MG, Vidili G, Porcu A, Solinas A, Cigliano A, Pes GM, Ribback S, Dombrowski F, Chen X, Li L, and Calvisi DF (2017) Both de novo synthetized and exogenous fatty acids support the growth of hepatocellular carcinoma cells. *Liver Int* **37**: 80-89.

Cerhan JR, Torner JC, Lynch CF, Rubenstein LM, Lemke JH, Cohen MB, Lubaroff DM, and Wallace RB (1997) Association of smoking, body mass, and physical activity with risk of prostate cancer in the Iowa 65+ Rural Health Study (United States). *Cancer Causes Control* **8**: 229-238.

Connolly JM, Coleman M, and Rose DP (1997) Effects of dietary fatty acids on DU145 human prostate cancer cell growth in athymic nude mice. *Nutr Cancer* **29**: 114-119.

Cozzo AJ, Fuller AM, and Makowski L (2017) Contribution of adipose tissue to development of cancer. *Compr Physiol* **8**: 237-282.

Daniels VW, Smans K, Royaux I, Chypre M, Swinnen JV, and Zaidi N (2014) Cancer cells differentially activate and thrive on de novo lipid synthesis pathways in a low-lipid environment. *PLoS One* **9**: e106913.

De Schrijver E, Brusselmans K, Heyns W, Verhoeven G, and Swinnen JV (2003) RNA interference-mediated silencing of the fatty acid synthase gene attenuates growth and induces morphological changes and apoptosis of LNCaP prostate cancer cells. *Cancer Res* **63**: 3799-3804.

Dean EJ, Falchook GS, Patel MR, Brenner AJ, Infante JR, Arkenau HT, Borazanci EH Lopez JS, Pant S, Schmid P, Frankel AE, Jones SF, McCulloch W, Kemble G, O'Farrell M, and Burris H (2016) Preliminary activity in the first in human study of the first-in-class fatty acid synthase (FASN) inhibitor, TVB-2640. *J Clin Oncology* **34**: 2512-2512.

Doak BC, Over B, Giordanetto F, and Kihlberg J (2014) Oral druggable space beyond the rule of 5: insights from drugs and clinical candidates. *Chem & Biol* **21**: 1115-1142.

Egan WJ, Merz KM, and Baldwin JJ (2000) Prediction of drug absorption using multivariate statistics. *J Med Chem* **43**: 3867-3877.

Fair WR, Fleshner NE, and Heston W (1997) Cancer of the prostate: a nutritional disease? *Urology* **50**: 840-848.

Flavin R, Peluso S, Nguyen PL, and Loda M (2010) Fatty acid synthase as a potential therapeutic target in cancer. *Future Oncol* **6**: 551-562.

Gazi E, Gardner P, Lockyer NP, Hart CA, Brown MD, and Clarke NW (2007) Direct evidence of lipid translocation between adipocytes and prostate

cancer cells with imaging FTIR microspectroscopy. *J Lipid Res* **48**: 1846-1856.

Gonzalez-Guerrico AM, Espinoza I, Schroeder B, Park CH, Kvp CM, Khurana A, Corominas-Faja B, Cuyas E, Alarcon T, Kleer C, Menendez JA, and Lupu R (2016) Suppression of endogenous lipogenesis induces reversion of the malignant phenotype and normalized differentiation in breast cancer. *Oncotarget* **7**: 71151-71168.

Gonzalez-Reyes C, Marcial-Medina C, Cervantes-Anaya N, Cortes-Reynosa P, and Salazar EP (2018) Migration and invasion induced by linoleic acid are mediated through fascin in MDA-MB-231 breast cancer cells. *Mol Cell Biochem* **443**: 1-10.

Hajduk PJ, Bures M, Praestgaard J, and Fesik SW (2000) Privileged molecules for protein binding identified from NMR-based screening. *J Med Chem* **43**: 3443-3447.

Hanahan D, and Weinberg RA (2011) Hallmarks of cancer: the next generation. *Cell* **144**: 646-674.

Heuer TS, Ventura R, Mordec K, Lai J, Fridlib M, Buckley D, and Kemble G (2017) FASN inhibition and taxane treatment combine to enhance anti-tumor efficacy in diverse xenograft tumor models through disruption of tubulin palmitoylation and microtubule organization and FASN inhibition-mediated effects on oncogenic signaling and gene expression. *EBioMedicine* **16**: 51-62.

Institute (National Cancer Institute) (2017) FASN inhibitor TVB-2640 in treating patients with colon or other cancers that can be removed by surgery. Accessed April 5, 2019: https://www.cancer.gov/about-cancer/treatment/clinical-trials/search/v?id=NCI-2016-01710&r=1

Jafari N, Drury J, Morris AJ, Onono FO, Stevens PD, Gao T, Liu J, Wang C, Lee EY, Weiss HL, Evers BM, and Zaytseva YY (2019) De novo fatty acid synthesis driven sphingolipid metabolism promotes metastatic potential of colorectal cancer. *Mol Cancer Res* **17**: 140-152.

Jung YY, Kim HM, and Koo JS (2015) Expression of lipid metabolism-related proteins in metastatic breast cancer. *PLoS One* **10**: e0137204.

Keller PM, Rust T, Murphy DJ, Matico R, Trill JJ, Krawiec JA, and Schwartz B (2008) A high-throughput screen for endothelial lipase using HDL as substrate. *J Biomol Screen* **13**, 468-475.

Kinlaw WB, Baures PW, Lupien LE, Davis WL, and Kuemmerle NB (2016) Fatty acids and breast cancer: Make them on site or have them delivered. *J Cell Physiol* **231**: 2128-2141.

Kridel SJ, Axelrod F, Rozenkrantz N, and Smith JW (2004) Orlistat is a novel inhibitor of fatty acid synthase with antitumor activity. *Cancer Res* **64**: 2070-2075.

Kuemmerle NB, Rysman E, Lombardo PS, Flanagan AJ, Lipe BC, Wells WA, Pettus JR, Froehlich HM, Memoli VA, Morganelli PM, Swinnen JV, Timmerman LA, Chaychi L, Fricano CJ, Eisenberg BL, Coleman WB, and

Kinlaw WB (2011) Lipoprotein lipase links dietary fat to solid tumor cell proliferation. *Mol Cancer Ther* **10**: 427-436.

Kuhajda FP, Jenner K, Wood FD, Hennigar RA, Jacobs LB, Dick JD, and Pasternack GR (1994) Fatty acid synthesis: a potential selective target for antineoplastic therapy. *Proc Natl Acad Sci U S A* **91**: 6379-6383.

Lagorce D (2018) from http://fafdrugs4.mti.univ-paris-diderot.fr.

Lagorce D, Sperandio O, Galons H, Miteva MA, and Villoutreix BO (2008) FAF-Drugs2: free ADME/tox filtering tool to assist drug discovery and chemical biology projects. *BMC Bioinformatics* **9**: 396.

Levental I, Lingwood D, Grzybek M, Coskun U, and Simons K (2010) Palmitoylation regulates raft affinity for the majority of integral raft proteins. *Proc Natl Acad Sci U S A* **107**: 22050-22054.

Li J, and Cheng JX (2014) Direct visualization of de novo lipogenesis in single living cells. *Sci Rep* **4**: 6807.

Li L, Che L, Tharp KM, Park HM, Pilo MG, Cao D, Cigliano A, Latte G, Xu Z, Ribback S, Dombrowski F, Evert M, Gores GJ, Stahl A, Calvisi DF, and Chen X (2016) Differential requirement for de novo lipogenesis in cholangiocarcinoma and hepatocellular carcinoma of mice and humans. *Hepatology* **63**: 1900-1913.

Lipinski CA, Lombardo F, Dominy BW, and Feeney PF (1997) Experimental and computational approaches to estimate solubility and permeability in drug discovery and development settings. *Adv Drug Deliv Rev* **23**: 3-25.

Lipinski CA (2000) Drug-like properties and the causes of poor solubility and poor permeability. *J Pharmacol Toxicol Meth* **44**: 235-249.

Lipinski CA (2004) Lead- and drug-like compounds: the rule-of-five revolution. *Drug Discov Today Technol* **1**: 337-341.

Liu H, Liu Y, and Zhang JT (2008) A new mechanism of drug resistance in breast cancer cells: fatty acid synthase overexpression-mediated palmitate overproduction. *Mol Cancer Ther* **7**: 263-270.

Liu H, Liu JY, Wu X, and Zhang JT (2010) Biochemistry, molecular biology, and pharmacology of fatty acid synthase, an emerging therapeutic target and diagnosis/prognosis marker. *Int J Biochem Mol Biol* **1**: 69-89.

Liu H, Wu X, Dong Z, Luo Z, Zhao Z, Xu Y, and Zhang JT (2013) Fatty acid synthase causes drug resistance by inhibiting TNF-alpha and ceramide production. *J Lipid Res* **54**: 776-785.

Luo X, Cheng C, Tan Z, Li N, Tang M, Yang L, and Cao Y (2017) Emerging roles of lipid metabolism in cancer metastasis. *Mol Cancer* **16**: 76.

Luo G, He Y, and Yu X (2018) Bone marrow adipocyte: an intimate partner with tumor cells in bone metastasis. *Front Endocrinol (Lausanne)* **9**: 339.

Massa M, Gasparini S, Baldelli I, Scarabelli L, Santi P, Quarto R, and Repaci E (2016) Interaction between breast cancer cells and adipose tissue cells derived from fat grafting. *Aesthet Surg J* **36**: 358-363.

Menendez JA, Vellon L, and Lupu R (2005) Targeting fatty acid synthase-driven lipid rafts: a novel strategy to overcome trastuzumab resistance in breast cancer cells. *Med Hypotheses* **64**: 997-1001.

Menendez JA, and Lupu R (2007) Fatty acid synthase and the lipogenic phenotype in cancer pathogenesis. *Nat Rev Cancer* **7**: 763-777.

Menendez JA, and Lupu R (2017) Fatty acid synthase (FASN) as a therapeutic target in breast cancer. *Expert Opin Ther Targets* **21**: 1001-1016.

Narita S, Tsuchiya N, Saito M, Inoue T, Kumazawa T, Yuasa T, Nakamura A, and Habuchi T (2008) Candidate genes involved in enhanced growth of human prostate cancer under high fat feeding identified by microarray analysis. *Prostate* **68**: 321-335.

Nieman KM, Romero IL, Van Houten B, and Lengyel E (2013) Adipose tissue and adipocytes supports tumorigenesis and metastasis. *Biochim Biophys Acta* **1831**: 1533-1541.

Nomura D, and Casida J. (2016) Lipases and their inhibitors in health and disease. *Chem Biol Interact* **259**: 211-222.

Notarnicola M, Miccolis A, Tutino V, Lorusso D, and Caruso MG (2012) Low levels of lipogenic enzymes in peritumoral adipose tissue of colorectal cancer patients. *Lipids* **47**: 59-63.

Pemble IV CW, Johnson LC, Kridel SJ, and Lowther WT (2007) Crystal structure of the thioesterase domain of human fatty acid synthase inhibited by Orlistat. *Nat Struct Mol Biol* **14**: 704.

Perchellet EM, Perchellet JP, and Baures PW (2005) Imidazole-4,5-dicarboxamide derivatives with antiproliferative activity against HL-60 cells. *J Med Chem* **48**: 5955-5965.

Pizer ES, Jackisch C, Wood FD, Pasternack GR, Davidson NE, and Kuhajda FP (1996) Inhibition of fatty acid synthesis induces programmed cell death in human breast cancer cells. *Cancer Res* **56**: 2745-2747.

Proschak E, Heitel P, Kalinowsky L, and Merk D (2017) Opportunities and challenges for fatty acid mimetics in drug discovery. *J Med Chem* **60**: 5235-5266.

Rohrig F, and Schulze A (2016) The multifaceted roles of fatty acid synthesis in cancer. *Nat Rev Cancer* **16**: 732-749.

Rozovski U, Grgurevic S, Bueso-Ramos C, Harris DM, Li P, Liu Z, Wu JY, Jain P, Wierda W, Burger J, O'Brien S, Jain N, Ferrajoli A, Keating MJ, and Estrov Z (2015) Aberrant LPL expression, driven by STAT3, mediates free fatty acid metabolism in CLL cells. *Mol Cancer Res* **13**: 944-953.

Rozovski U, Hazan-Halevy I, Barzilai M, Keating MJ, and Estrov Z (2016) Metabolism pathways in chronic lymphocytic leukemia. *Leuk Lymphoma* **57**: 758-765.

Rozovski U, Harris DM, Li P, Liu Z, Jain P, Ferrajoli A, Burger J, Thompson P, Jain N, Wierda W, Keating MJ, and Estrov Z (2018) STAT3-activated CD36 facilitates fatty acid uptake in chronic lymphocytic leukemia cells. *Oncotarget* **9**: 21268-21280.

Ruby MA, Goldenson B., Orasanu G, Johnston TP, Plutzky J, and Krauss RM (2010) VLDL hydrolysis by LPL activates PPAR-alpha through generation of unbound fatty acids. *J Lipid Res* **51**: 2275-2281.

Rush JR, Sandstrom SL, Yang J, Davis R, Prakash O, and Baures PW (2005) Intramolecular hydrogen bond strength and pKa determination of *N*, *N*'-disubstituted imidazole-4,5-dicarboxamides. *Org Lett* **7**: 135-138.

Rysman E, Brusselmans K, Scheys K, Timmermans L, Derua R, Munck S, Van Veldhoven PP, Waltregny D, Daniels VW, Machiels J, Vanderhoydonc F, Smans K, Waelkens E, Verhoeven G, and Swinnen JV (2010) De novo lipogenesis protects cancer cells from free radicals and chemotherapeutics by promoting membrane lipid saturation. *Cancer Res* **70**: 8117-8126.

Schug ZT, Peck B, Jones DT, Zhang Q, Grosskurth S, Alam IS, Goodwin LM, Smethurst E, Mason S, Blyth K, McGarry L, James D, Shanks E, Kalna G, Saunders RE, Jiang M, Howell M, Lassailly F, Thin MZ, Spencer-Dene B, Stamp G, van den Broek NJ, Mackay G, Bulusu V, Kamphorst JJ, Tardito S, Strachan D, Harris AL, Aboagye EO, Critchlow SE, Wakelam MJ, Schulze A, and Gottlieb E (2015) Acetyl-CoA synthetase 2 promotes acetate utilization and maintains cancer cell growth under metabolic stress. *Cancer Cell* **27**: 57-71.

Singh R, Yadav V, Kumar S, and Saini N (2015) MicroRNA-195 inhibits proliferation, invasion and metastasis in breast cancer cells by targeting FASN, HMGCR, ACACA and CYP27B1. *Sci Rep* **5**: 17454.

Slebe F, Rojo F, Vinaixa M, Garcia-Rocha M, Testoni G, Guiu M, Planet E, Samino S, Arenas EJ, Beltran A, Rovira A, Lluch A, Salvatella X, Yanes O, Albanell J, Guinovart JJ, and Gomis RR (2016) FoxA and LIPG endothelial

lipase control the uptake of extracellular lipids for breast cancer growth. *Nat Commun* **7**: 11199.

Solinas R, DiCesare JC, and Baures PW (2008) Parallel synthesis of an imidazole-4,5-dicarboxamide library bearing amino acid esters and alkanamines. *Molecules* **13**: 3149-3170.

Solinas R, DiCesare JC and Baures PW (2009) Parallel synthesis of a library of symmetrically-and dissymmetrically-disubstituted imidazole-4,5-dicarboxamides bearing amino acid esters. *Molecules* **14**: 352-363.

Song HJ, Sneddon AA, Heys SD, and Wahle KW (2012) Regulation of fatty acid synthase (FAS) and apoptosis in estrogen-receptor positive and negative breast cancer cells by conjugated linoleic acids. *Prostaglandins Leukot Essent Fatty Acids* **87**: 197-203.

Sundaram S, Zacek P, Bukowski MR, Mehus AA, Yan L, and Picklo MJ (2018) Lipidomic Impacts of an Obesogenic Diet Upon Lewis Lung Carcinoma in Mice. *Front Oncol* **8**: 134.

Svensson RU, Parker SJ, Eichner LJ, Kolar MJ, Wallace M, Brun SN, Lombardo PS, Van Nostrand JL, Hutchins A, Vera L, Gerken L, Greenwood J, Bhat S, Harriman G, Westlin WF, Harwood Jr. HJ, Saghatelian A, Kapeller R, Metallo CM, and Shaw RJ (2016) Inhibition of acetyl-CoA carboxylase suppresses fatty acid synthesis and tumor growth of non-small-cell lung cancer in preclinical models. *Nat Med* **22**: 1108-1119.

Swinnen JV, Van Veldhoven PP, Timmermans L, De Schrijver E, Brusselmans K, Vanderhoydonc F, Van de Sande T, Heemers H, Heyns W, and Verhoeven

G (2003) Fatty acid synthase drives the synthesis of phospholipids partitioning into detergent-resistant membrane microdomains. *Biochem Biophys Res Commun* **302**: 898-903.

Tang FY, Pai MH, and Chiang EP (2012) Consumption of high-fat diet induces tumor progression and epithelial-mesenchymal transition of colorectal cancer in a mouse xenograft model. *J Nutr Biochem* **23**: 1302-1313.

Tokuda Y, Satoh Y, Fujiyama C, Toda S, Sugihara H and Masaki Z (2003) Prostate cancer cell growth is modulated by adipocyte-cancer cell interaction. *BJU Int* **91**: 716-720.

VanCompernolle SE, Wiznycia AV, Rush JR, Dhanasekaran M, Baures PW, and Todd SC (2003) Small molecule inhibition of hepatitis C virus E2 binding to CD81. *Virology* **314**: 371-380.

Vasseur S, and Guillaumond F (2016) LDL Receptor: An open route to feed pancreatic tumor cells. *Molecular & Cellular Oncology* **3**: e1033586.

Veber DF, Johnson SR, Cheng HY, Smith BR, Ward KW, and Kopple KD (2002) Molecular properties that influence the oral bioavailability of drug candidates. *J Med Chem* **45**: 2615-2623.

Ventura R, Mordec K, Waszczuk J, Wang Z, Lai J, Fridlib M, Buckley D, Kemble G, and Heuer TS (2015) Inhibition of de novo palmitate synthesis by fatty acid synthase induces apoptosis in tumor cells by remodeling cell membranes, inhibiting signaling pathways, and reprogramming gene expression. *EBioMedicine* **2**: 808-824.

Wagner R, Stubiger G, Veigel D, Wuczkowski M, Lanzerstorfer P, Weghuber J, Karteris E, Nowikovsky K, Wilfinger-Lutz N, Singer CF, Colomer R, Benhamu B, Lopez-Rodriguez ML, Valent P, and Grunt TW (2017) Multi-level suppression of receptor-PI3K-mTORC1 by fatty acid synthase inhibitors is crucial for their efficacy against ovarian cancer cells. *Oncotarget* **8**: 11600-11613.

Wang Y, Corr JG, Thaler HT, Tao Y, Fair WR, and Heston WD (1995) Decreased growth of established human prostate LNCaP tumors in nude mice fed a low-fat diet. *J Natl Cancer Inst* **87**: 1456-1462.

Wang H, Xi Q, and Wu G (2016) Fatty acid synthase regulates invasion and metastasis of colorectal cancer via Wnt signaling pathway. *Cancer Med* **5**: 1599-1606.

Warburg O (1956) On the origin of cancer cells. *Science* **123**: 309-314.

Ward PS, and Thompson CB (2012) Metabolic reprogramming: a cancer hallmark even warburg did not anticipate. *Cancer Cell* **21**: 297-308.

Wu X, Qin L, Fako V, and Zhang JT (2014) Molecular mechanisms of fatty acid synthase (FASN)-mediated resistance to anti-cancer treatments. *Adv Biol Regul* **54**: 214-221.

Zaidi N, Lupien L, Kuemmerle NB, Kinlaw WB, Swinnen JV, and K. Smans K (2013) Lipogenesis and lipolysis: the pathways exploited by the cancer cells to acquire fatty acids. *Prog Lipid Res* **52**: 585-589.

Zaidi N, Royaux I, Swinnen JV, and Smans K (2012) ATP citrate lyase knockdown induces growth arrest and apoptosis through different cell- and environment-dependent mechanisms. *Mol Cancer Ther* **11**: 1925-1935.

Zaytseva YY, Rychahou PG, Gulhati P, Elliott VA, Mustain WC, O'Connor K, Morris AJ, Sunkara M, Weiss HL, Lee EY, and Evers BM (2012) Inhibition of fatty acid synthase attenuates CD44-associated signaling and reduces metastasis in colorectal cancer. *Cancer Res* **72**: 1504-1517.

Zaytseva YY, Elliott VA, Rychahou P, Mustain WC, Kim JT, Valentino J, Gao T, O'Connor KL, Neltner JM, Lee EY, Weiss HL, and Evers BM (2014) Cancer cell-associated fatty acid synthase activates endothelial cells and promotes angiogenesis in colorectal cancer. *Carcinogenesis* **35**: 1341-1351.

Footnotes

This research was made possible by the Institutional Development Award (IDeA) Program of the National Institutes of Health National Institute of General Medical Sciences [Grant P20GM103506] to PWB and WBK as well as a National Institutes of Health National Cancer Institute grant [R01CA58961] to WBK. This research was also supported by the National Institutes of Health National Cancer Institute [P30CA023108] for LDL and DBP. Support to PWB for the KSC NMR Facility [National Science Foundation 1337206] is appreciated, as is support from The Friends of Norris Cotton Cancer Center to PWB and WBK.

[1]The confirmatory bioassays can be viewed in PubChem by searching AID 624326 or AID 624327 under PubChem Bioassay. The SID number for **1** is 49733438. Direct links to the confirmatory bioassay data for **1** are as follows:

https://pubchem.ncbi.nlm.nih.gov/bioassay/624326#sid=49733438

https://pubchem.ncbi.nlm.nih.gov/bioassay/624327#sid=49733438

[2]The original bioassay can be viewed in PubChem by searching AID 602261 under PubChem Bioassay. The SID number for **15** is 24833677. A direct link to the bioassay data for **15** is as follows:

https://pubchem.ncbi.nlm.nih.gov/bioassay/602261#sid=24833677&section=Top

[3]The SID number for **9** is 26724152. Direct links to the confirmatory bioassay data for **9** are as follows:

https://pubchem.ncbi.nlm.nih.gov/bioassay/624326#sid=26724152

https://pubchem.ncbi.nlm.nih.gov/bioassay/624327#sid=26724152

JPET Fast Forward. Published on July 12, 2019 as DOI: 10.1124/jpet.119.258947
This article has not been copyedited and formatted. The final version may differ from this version.

Figure Legends

Figure 1. SAR summary of *N*,*N*'-disubstituted imidazole-4,5-dicarboxamides active in confirmatory screens against FASN-TE.

Figure 2. Structure, cytotoxicity, and mouse plasma stability data for 11-14. (**A**) Structure of derivatives that modify the ester bond of **1**. (**B**, **C**) MCF-7 BC cells were treated with FASNi for 72 h in standard media and assessed using the alamarBlue cell viability assay. (**B**) Concentration-response curves for compounds **11-14**. Data are presented as mean +/- SD (N = 3-5 experiments). Here and in all ensuing figures, IC_{50} values were generated using a non-linear regression curve-fitting algorithm: log(inhibitor) vs. response-variable slope (four parameter) with Graph Pad Prism 6.0. (**C**) Compiled IC_{50} and mouse plasma stability results, represented by percent compound remaining after 1 h incubation in mouse plasma at 37°C (N.D., not determined).

Figure 3. Structure of ester-to-amide derivatives of **1** along with methyl groups that add steric bulk.

Figure 4. Structure, cytotoxicity and mouse plasma stability data for 25-37. (**A**) Benzylamine derivatives **25-37**: structure, compiled IC_{50} and mouse plasma stability results, represented by percent compound remaining after 1 h incubation in mouse plasma at 37°C. (**B**, **C**) Cytotoxicity concentration-response curves for

25-**37** against MCF-7 BC cells following 72 h continuous treatment in standard media, assessed using the alamarBlue cell viability assay, N = 2-5 experiments. Data shown as mean +/- SD.

Figure 5. Structure, cytotoxicity and mouse plasma stability data for 9, 38-43. (**A**) Structural comparison of cyclohexylamine derivatives based on **9**. (**B**) Cytotoxicity of **38**-**43** against MCF-7 BC cells following 72 h continuous treatment in standard media, assessed using the alamarBlue cell viability assay, N = 4-6 experiments. (**C**) Compiled IC_{50} and mouse plasma stability results, represented by percent compound remaining after 1 h incubation in mouse plasma at 37°C.

Figure 6. Cytotoxicity and stability of promising cyclohexylamine derivatives (38, 39, 41, 42). (**A**) Cell viability was assessed using the ATP-based CTG assay following 72 h continuous treatment with FASNi in standard media. A comparison of the concentration-response trends generated for each FASNi in three different BC cell lines (MCF-7, MDA-MB-231, BT-474), N = 2-5 experiments per compound. (**B**) Compiled IC_{50} values for each of the four FASNi. (**C**) Viability of non-cancerous MCF10A mammary epithelial cells following 72 h treatment with FASNi in standard media. Data not fitted to a nonlinear curve. (**D**) Compound stability represented as % recovery compared to control compound (**ILP-III-15**).

JPET Fast Forward. Published on July 12, 2019 as DOI: 10.1124/jpet.119.258947
This article has not been copyedited and formatted. The final version may differ from this version.

Figure 7. On-target inhibition of FASN by 41. (**A**) Treatment of BT-474 lipogenic, HER2+ BC cells with **41** (4 h, 50 μM) directly inhibited FASN activity, as shown by a significant accumulation of the committed substrate for *de novo* lipogenesis, malonyl-CoA (*$p < 0.05$, one-way Anova; biological duplicate, technical triplicate samples). (**B**) The ability of **1** and **41** to specifically target the thioesterase domain of FASN was assessed using a FASN-TE substrate hydrolysis assay (N = 3 experiments). Under these conditions, the FASN-TE IC_{50} of **1** was 1.47 ± 0.17 μM with a Hill slope of 0.773, whereas that of **41** was 14.58 ± 1.16 μM with a Hill slope of 0.824.

Figure 8. Cytotoxicity of 41 exceeds that of (-)-C75 across a range of cancer cell lines. Cells were treated with FASNi continuously for 72 h in standard 10% FBS RPMI-1640 and assessed using the ATP-based CTG viability assay (**A**, **B**, **E**, **F**) or Annexin V/PI cell death/apoptosis assay (**C**, **D**). (**A**) Concentration-response curves for each BC cell line. (**B**) IC_{50} values for **41** vs. (-)-C75. (**C, D**) FASN inhibition causes concentration-dependent apoptosis in MDA-MB-231 and BT-474 BC cells, as detected by Annexin V/PI flow cytometry. The apoptosis observed with **41** treatment significantly exceeds that of (-)-C75 at several concentrations, as indicated. Two-tailed, unpaired t-tests were performed to compare the effects of (-)-C75 at equimolar concentrations, *$p \leq 0.05$, **$p \leq 0.01$, ***$p \leq 0.001$. (**E**) Compound **41** displays minimal cytotoxicity against MCF10A mammary epithelial cells. (**F**) Similar cytotoxicity trends observed across cancer cell lines; negligible

JPET Fast Forward. Published on July 12, 2019 as DOI: 10.1124/jpet.119.258947
This article has not been copyedited and formatted. The final version may differ from this version.

impact on MCF10A mammary epithelial cell viability. N ≥ 5 experiments for all treatments.

Figure 9. Availability of media lipoproteins impacts cytotoxicity and cell death from FASN inhibitor treatment. Increased cytotoxicity was observed with 72 h treatment of **41** in RPMI-1640 media containing 10% LPDS vs. the matched serum control. This trend was observed in all cell lines tested and reflected in both assessments of (**A**) cell viability (CTG) and (**B**) apoptosis (Annexin/PI flow cytometry). No significant differences in cell viability were observed in cells grown for 72 h in matched or LPDS media alone (not shown). N = 3-7 experiments per assay. Error expressed as SD from the mean, *p ≤ 0.05, **p ≤ 0.01, ***p ≤ 0.001.

Figure 10. Simultaneous inhibition of FA synthesis and uptake (via lipolysis) results in increased cytotoxicity of BC cells *in vitro.* (**A**) Continuous treatment with lipase inhibitor, GSK264220A, for 72 h resulted in concentration-dependent cytotoxicity in MDA-MB-231 and BT-474 BC cells, and is impacted by the presence of lipoproteins in the media at high concentrations (> 50 μM). (**B**) Simultaneously targeting FA synthesis and uptake using **41** and GSK264220A causes increased cytotoxicity in MDA-MB-231 and BT-474 BC cells. The effects of continuous combined treatments are compared to that of **41** alone (supplemented with DMSO to match the highest vehicle exposure). (**C**) The impact of media lipoproteins on the cytotoxic effects of **41** and combined treatments of **41** and GSK at 100 μM. Viability was measured using the ATP-

JPET Fast Forward. Published on July 12, 2019 as DOI: 10.1124/jpet.119.258947
This article has not been copyedited and formatted. The final version may differ from this version.

based CTG assay. For each (**B**) and (**C**), data points at a concentration of 0 μM compound **41** represent the relative viability of the vehicle control condition, or the effect of GSK alone (without FASNi present). N = 3-5 experiments for all treatments.

Figure 11. Physical-chemical parameters for 41 (intersects of the blue line) over the drug-like filter area for a lead compound (blue space). Abbreviations clockwise from top are as follows: HBA, number of hydrogen bond acceptors; tPSA, topological polar surface area; ratioH_C, ratio of hydrogen atoms to carbon atoms; n_hetero, total number of heteroatoms; n_carbon, total number of carbon atoms; n_SystemRing, smallest number of rings; logP, the logarithm of the partition coefficient between water and n-octanol; TotalCharge, formal charge of the compound; RotatableBonds, number of single non-ring bonds; RigidBonds, number of non-flexible bonds; NumCharges, number of charged groups; SizeSystemRing, number of atoms in the largest ring; MW, molecular weight; HBD, number of hydrogen bond donors.

JPET Fast Forward. Published on July 12, 2019 as DOI: 10.1124/jpet.119.258947
This article has not been copyedited and formatted. The final version may differ from this version.

Tables

Table 1. Immortalized human cell lines used in this study and their respective biomarker status and subtype, where applicable. ER (estrogen receptor), PR (progesterone receptor), HER2 (ErbB2).

Cell Line	Source	Tumor Type	Subtype	ER	PR	HER2
BT-474	Primary breast	Ductal carcinoma	Luminal B	+	+	+
DU4475	Mammary gland	Epithelial cell	TNBC, IM subtype	-	-	-
HeLa	Cervix	Adenocarcinoma	N/A			
MCF-7	Pleural effusion	Invasive ductal carcinoma	Luminal A	+	+	-
MCF10A	Primary breast	Epithelial cell	Basal	-	-	-
MDA-MB-231	Pleural effusion	Adenocarcinoma	Claudin-low or basal-like	-	-	-
LiSa-2	Pleomorphic liposarcoma	Liposarcoma	N/A		+	
SKBR3	Pleural effusion	Adenocarcinoma	Luminal	-	-	+
T47-D	Pleural effusion	Invasive ductal carcinoma	Luminal A	+	+	-

JPET Fast Forward. Published on July 12, 2019 as DOI: 10.1124/jpet.119.258947
This article has not been copyedited and formatted. The final version may differ from this version.

Schemes

Scheme 1

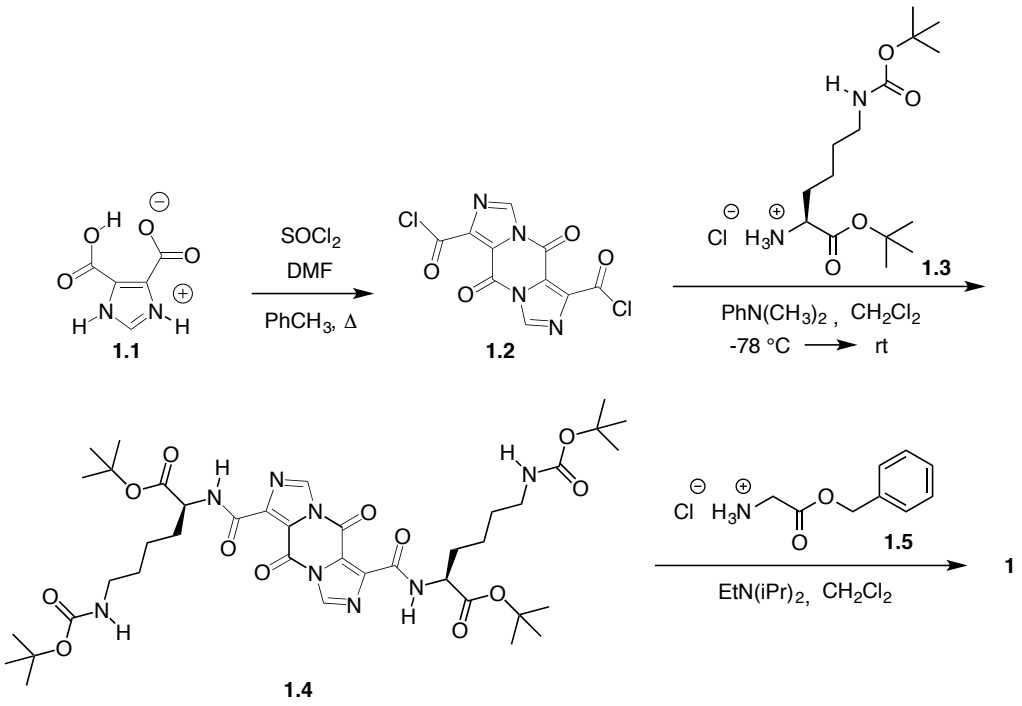

JPET Fast Forward. Published on July 12, 2019 as DOI: 10.1124/jpet.119.258947
This article has not been copyedited and formatted. The final version may differ from this version.

Figures

Figure 1

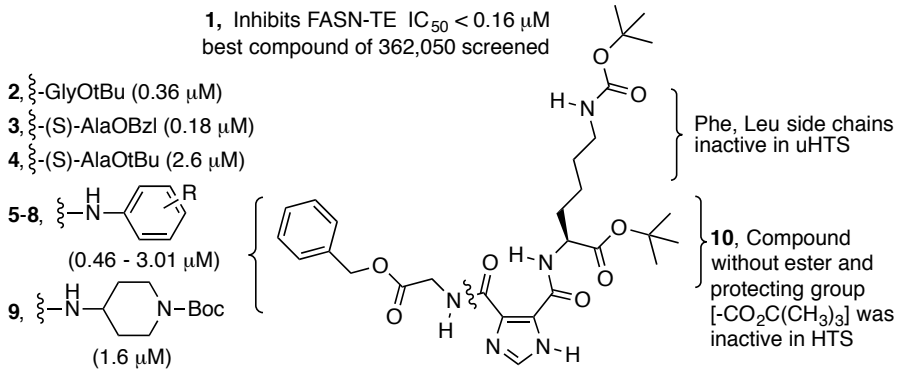

Figure 2

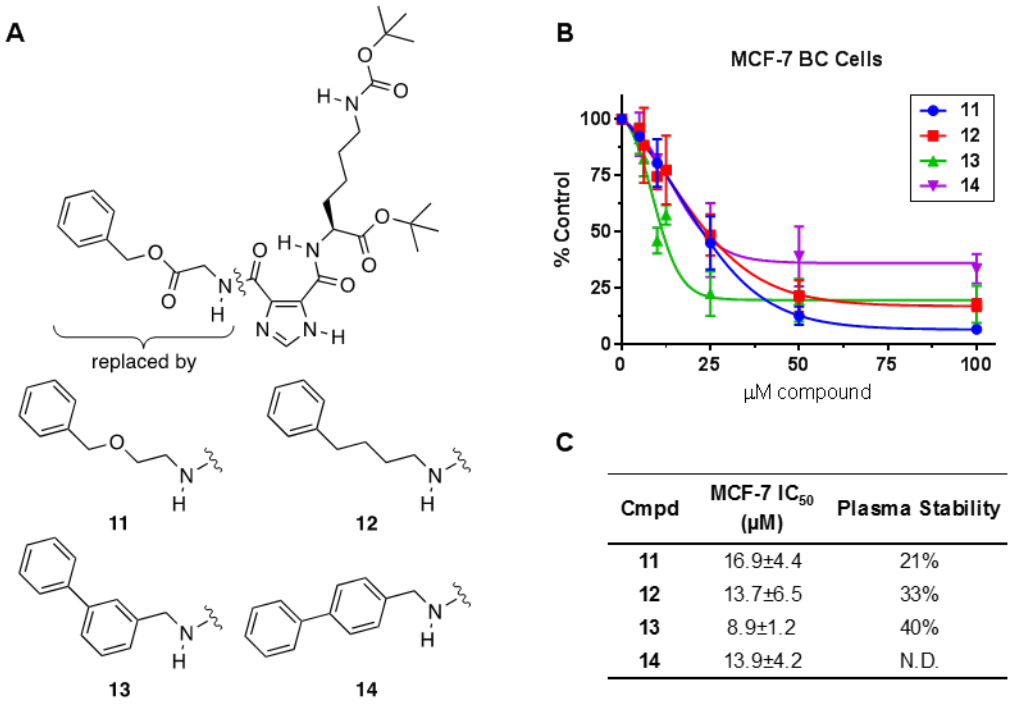

Cmpd	MCF-7 IC_{50} (μM)	Plasma Stability
11	16.9±4.4	21%
12	13.7±6.5	33%
13	8.9±1.2	40%
14	13.9±4.2	N.D.

JPET Fast Forward. Published on July 12, 2019 as DOI: 10.1124/jpet.119.258947
This article has not been copyedited and formatted. The final version may differ from this version.

JPET Fast Forward. Published on July 12, 2019 as DOI: 10.1124/jpet.119.258947
This article has not been copyedited and formatted. The final version may differ from this version.

Figure 3

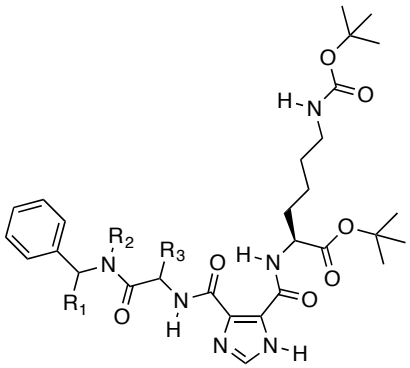

Cmpd	R_1	R_2	R_3
15	H	H	H
16	H	CH_3	H
17	*R*-(CH_3)	H	H
18	*S*-(CH_3)	H	H
19	H	H	*R*-(CH_3)
20	H	H	*S*-(CH_3)
21	H	CH_3	*R*-(CH_3)
22	H	CH_3	*S*-(CH_3)
23	*R*-(CH_3)	CH_3	H
24	*S*-(CH_3)	CH_3	H

JPET Fast Forward. Published on July 12, 2019 as DOI: 10.1124/jpet.119.258947
This article has not been copyedited and formatted. The final version may differ from this version.

Figure 4

A

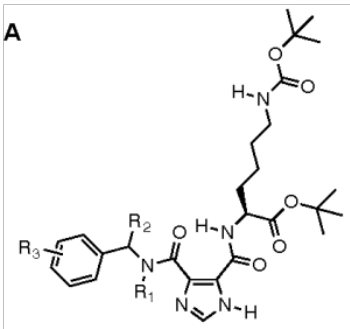

Cmpd	R_1	R_2	R_3	MCF-7 IC_{50} (μM)	Plasma Stability
25	H	H	H	20.0±0.8	21%
26	CH_3	H	H	23.8±3.9	65%
27	H	H	4-Cl	11.7±4.2	N.D.
28	H	H	3-Cl	10.0±0.9	N.D.
29	H	H	3-F,5-F	~10.2	N.D.
30	H	H	3-CH_3	8.5±6.2	6%
31	H	H	4-CH_3	18.9±2.7	27%
32	H	H	4-OCH_3	~45	N.D.
33	H	H	4-CH_2CH_3	~26	N.D.
34	H	H	4-$CH(CH_3)_2$	~20	N.D.
35	H	H	4-$C(CH_3)_3$	11.5±2.3	55%
36	CH_3	*S*-(CH_3)	H	~32	N.D.
37	CH_3	*R*-(CH_3)	H	ambigous	N.D.

B

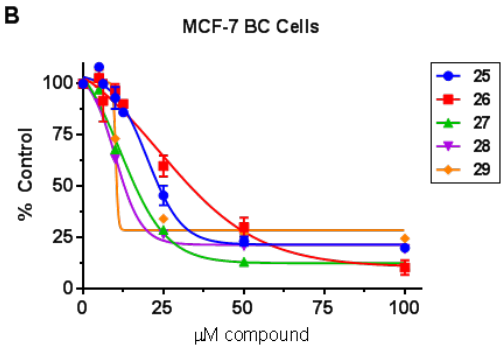

C

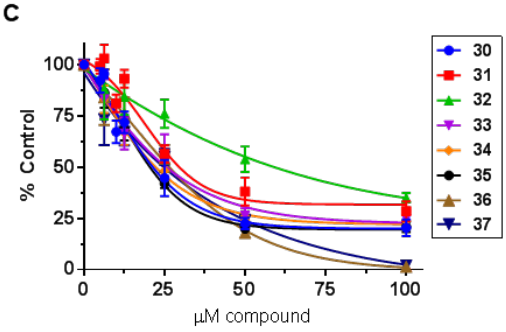

JPET Fast Forward. Published on July 12, 2019 as DOI: 10.1124/jpet.119.258947
This article has not been copyedited and formatted. The final version may differ from this version.

Figure 5

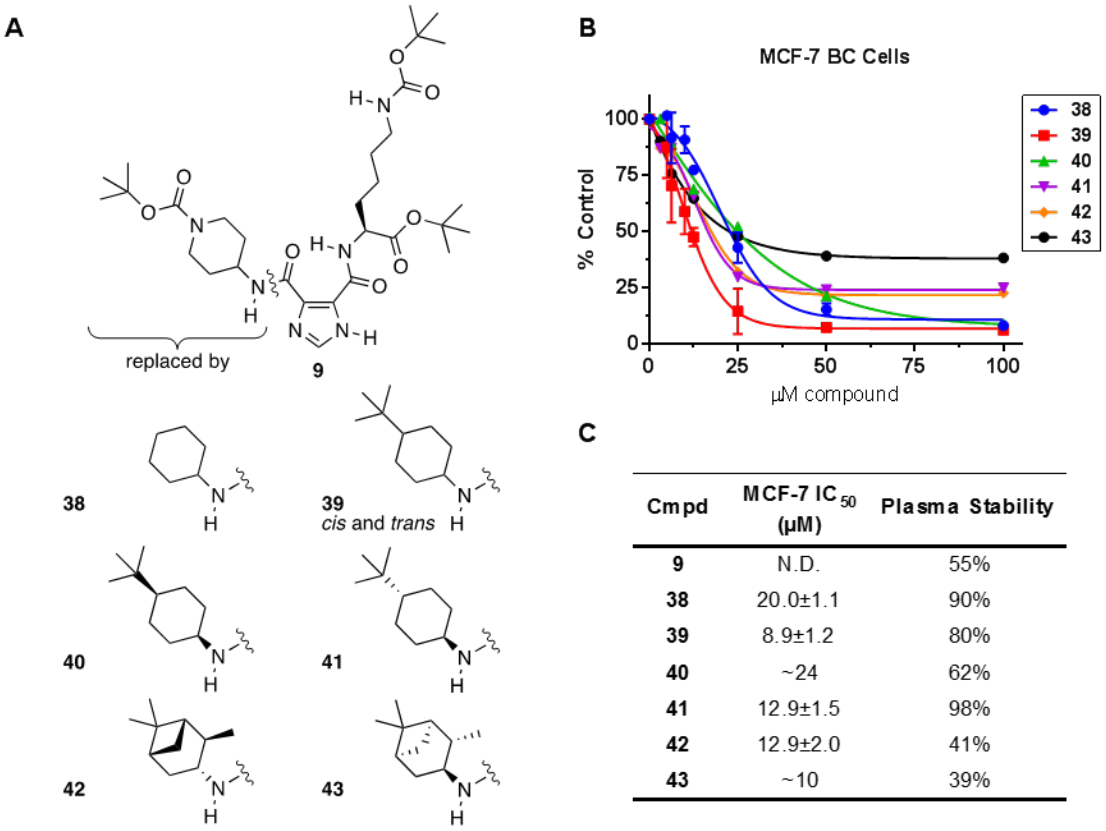

C

Cmpd	MCF-7 IC_{50} (µM)	Plasma Stability
9	N.D.	55%
38	20.0±1.1	90%
39	8.9±1.2	80%
40	~24	62%
41	12.9±1.5	98%
42	12.9±2.0	41%
43	~10	39%

JPET Fast Forward. Published on July 12, 2019 as DOI: 10.1124/jpet.119.258947
This article has not been copyedited and formatted. The final version may differ from this version.

Figure 6

A

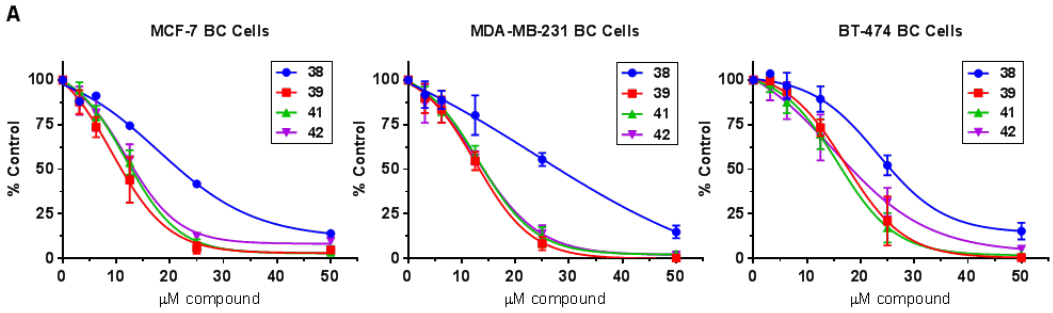

B

	FASNi IC_{50} Values (µM)			
Cell Line	**38**	**39**	**41**	**42**
MCF-7	21.5	12.0	13.4	13.6
MDA-MB-231	29.8	14.1	14.5	14.7
BT-474	26.5	17.3	16.5	18.6

C

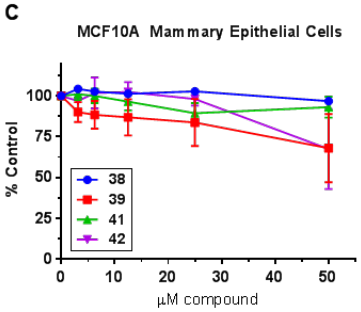

D

	Recovery (%)			
	38	**39**	**41**	**42**
Neat on Ice	99	100	100	100
Neat at RT	112	107	N.D.	N.D.
Neat at 37°C	111	121	99	85
Plasma on Ice	73	156	100	100
Plasma at RT	74	129	N.D.	N.D.
Plasma at 37°C	67	130	96	70

Figure 7

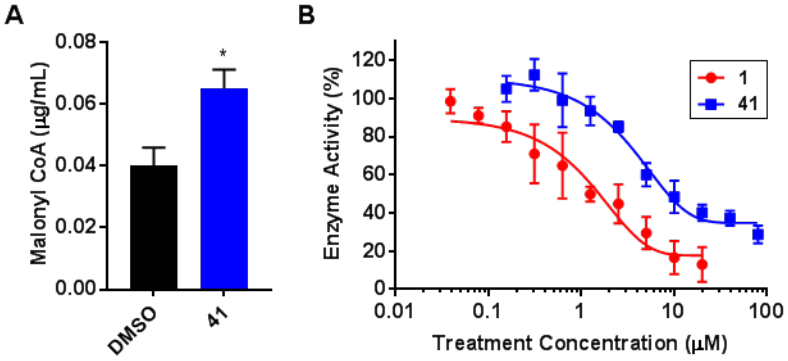

JPET Fast Forward. Published on July 12, 2019 as DOI: 10.1124/jpet.119.258947
This article has not been copyedited and formatted. The final version may differ from this version.

Figure 8

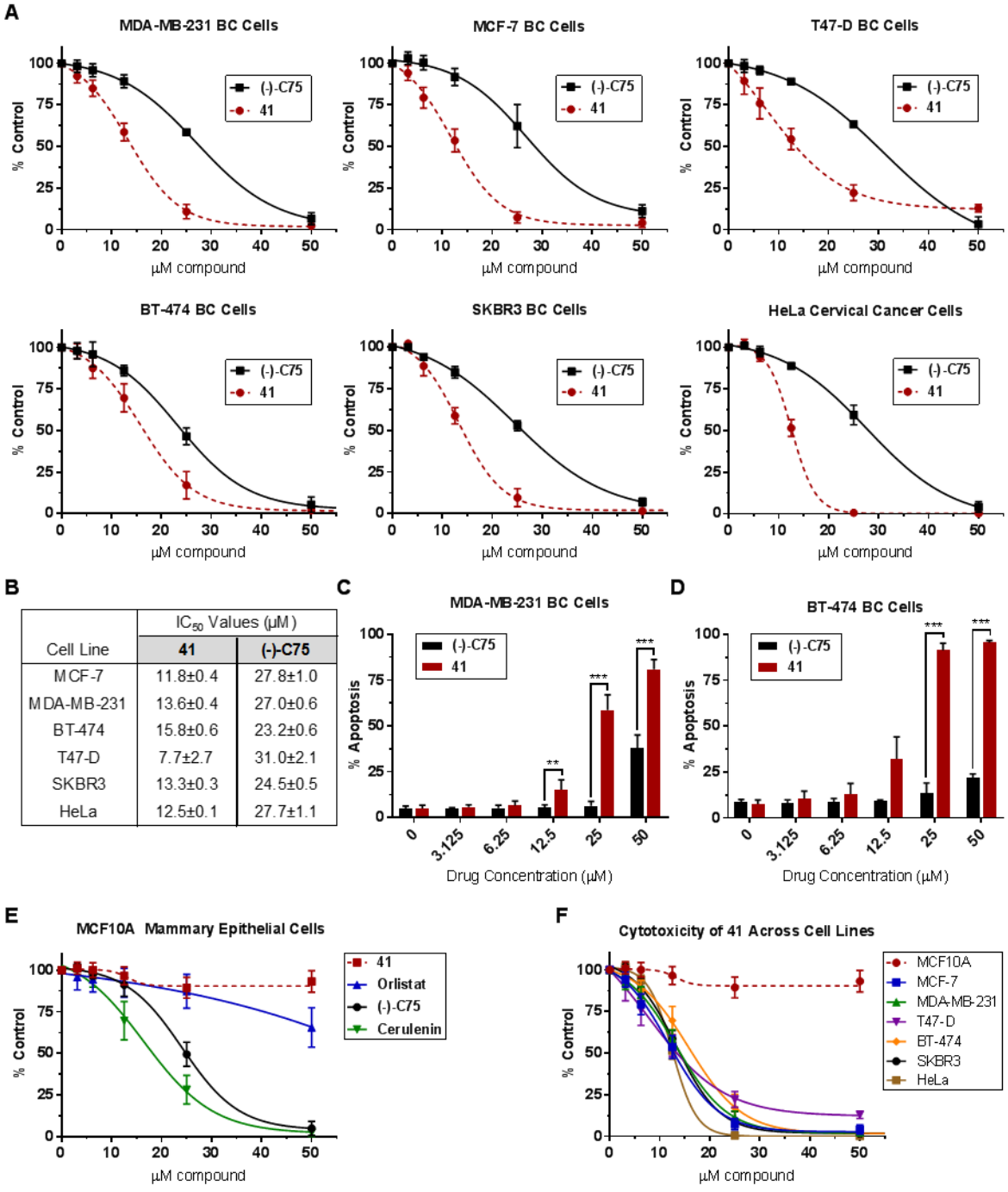

Cell Line	IC_{50} Values (µM)	
	41	(-)-C75
MCF-7	11.8±0.4	27.8±1.0
MDA-MB-231	13.6±0.4	27.0±0.6
BT-474	15.8±0.6	23.2±0.6
T47-D	7.7±2.7	31.0±2.1
SKBR3	13.3±0.3	24.5±0.5
HeLa	12.5±0.1	27.7±1.1

JPET Fast Forward. Published on July 12, 2019 as DOI: 10.1124/jpet.119.258947
This article has not been copyedited and formatted. The final version may differ from this version.

Figure 9

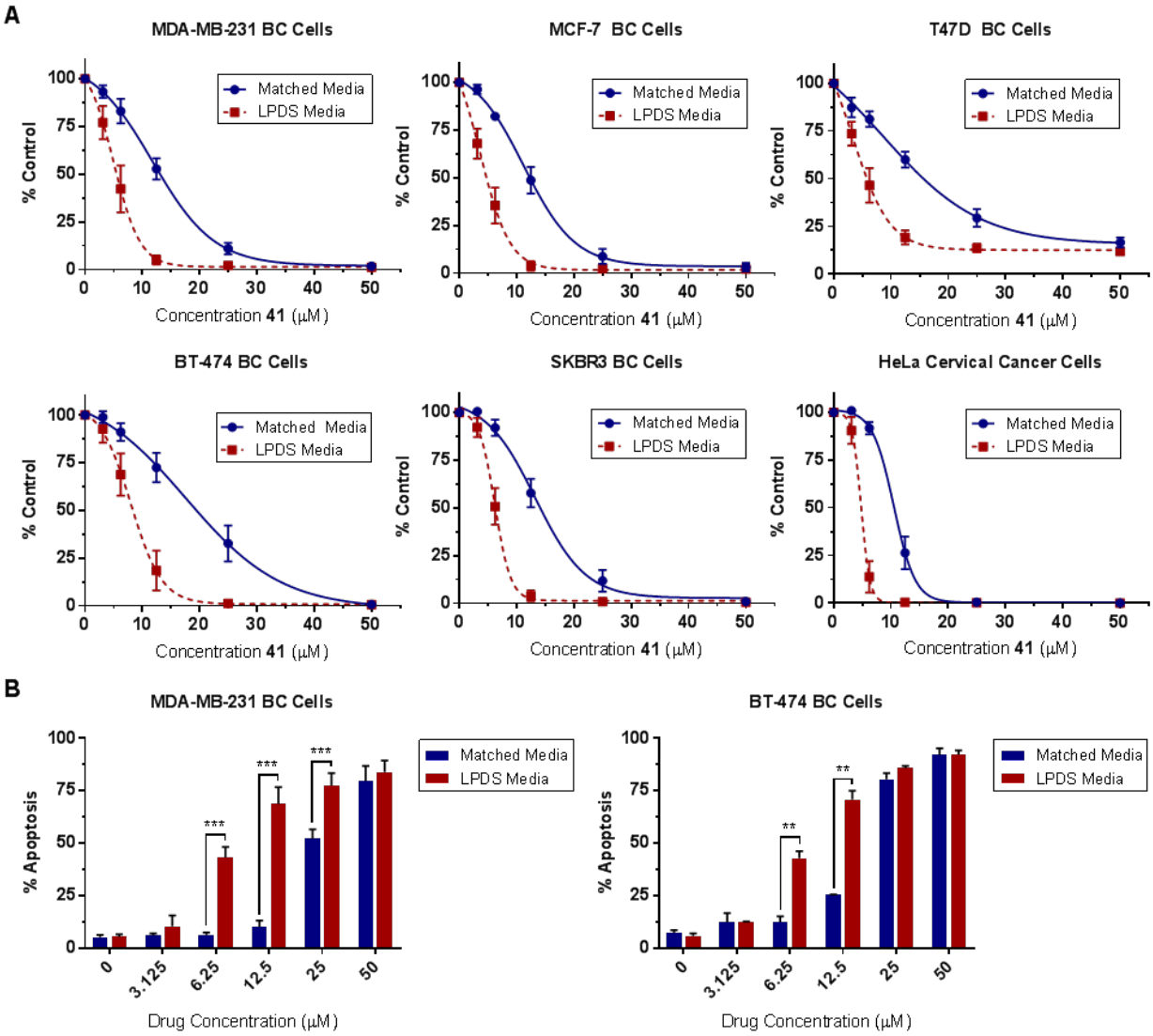

JPET Fast Forward. Published on July 12, 2019 as DOI: 10.1124/jpet.119.258947
This article has not been copyedited and formatted. The final version may differ from this version.

Figure 10

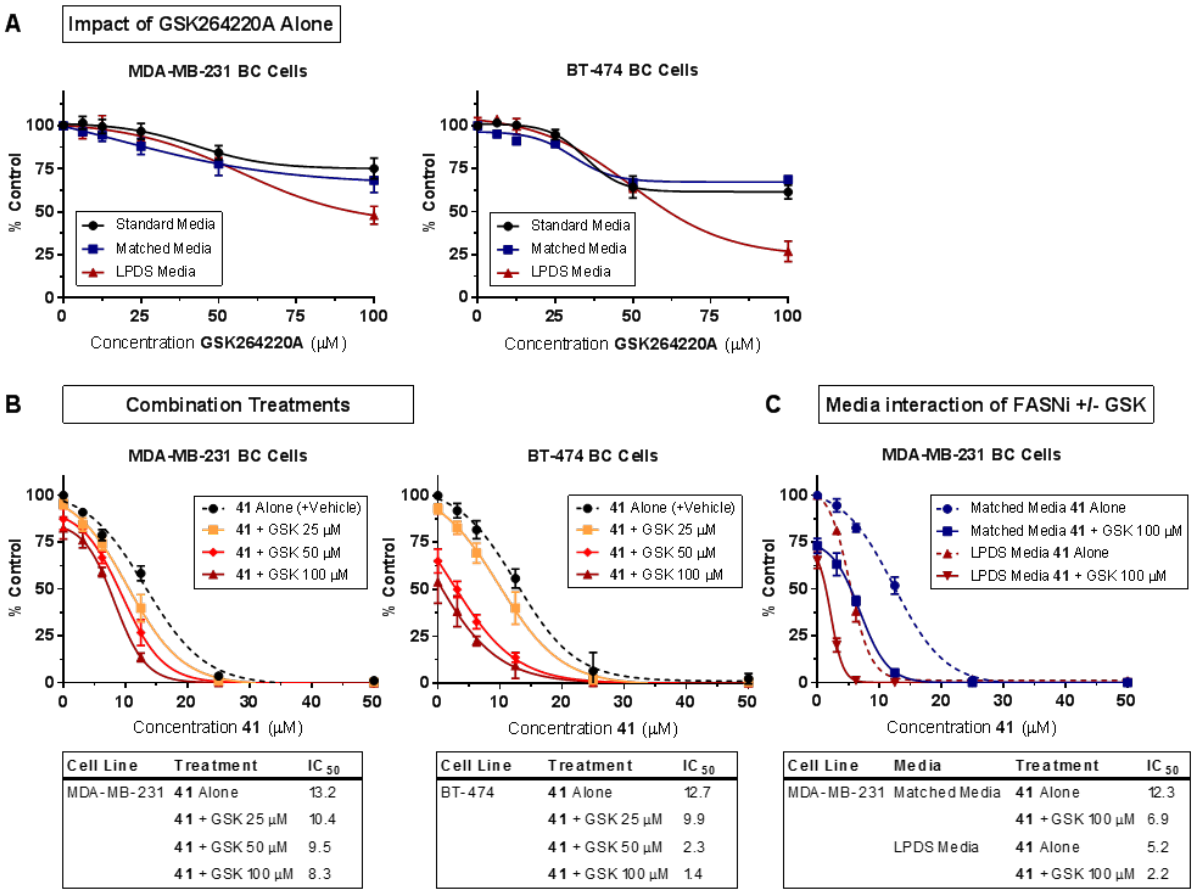

Cell Line	Treatment	IC_{50}
MDA-MB-231	**41** Alone	13.2
	41 + GSK 25 μM	10.4
	41 + GSK 50 μM	9.5
	41 + GSK 100 μM	8.3

Cell Line	Treatment	IC_{50}
BT-474	**41** Alone	12.7
	41 + GSK 25 μM	9.9
	41 + GSK 50 μM	2.3
	41 + GSK 100 μM	1.4

Cell Line	Media	Treatment	IC_{50}
MDA-MB-231	Matched Media	**41** Alone	12.3
		41 + GSK 100 μM	6.9
	LPDS Media	**41** Alone	5.2
		41 + GSK 100 μM	2.2

JPET Fast Forward. Published on July 12, 2019 as DOI: 10.1124/jpet.119.258947
This article has not been copyedited and formatted. The final version may differ from this version.

Figure 11